Microanalysis of carbonate cement $\delta^{18}O$ in a CO_2-storage system seal: Insights into the diagenetic history of the Eau Claire Formation (Upper Cambrian), Illinois Basin

Maciej G. Śliwiński, Reinhard Kozdon, Kouki Kitajima, Adam Denny, and John W. Valley

ABSTRACT

Oxygen isotope ($\delta^{18}O$) zonation in carbonate mineral cements is often employed as a proxy record (typically with millimeter-scale resolution) of changing temperature regimes during different stages of sediment diagenesis. Recent advances in secondary ion mass spectrometry allow for highly precise and accurate determinations of cement $\delta^{18}O$ values to be made in situ on a micrometer scale, thus significantly increasing the spatial resolution available to studies of diagenesis in sandstone–shale and carbonate systems. Chemo-isotopically zoned dolomite–ankerite cements within shaly sandstone beds of the predominantly silty–shaly Eau Claire Formation (Cambrian, Illinois Basin) were investigated, revealing the following: with increasing depth of burial (from <0.5 to ~2 km [<1500 to 6500 ft]), cement $\delta^{18}O$ values decrease from a high of approximately 24‰ down to approximately 14‰ (on the Vienna standard mean ocean water [VSMOW] scale, equivalent to –6.5‰ to –16.5‰ on the Vienna Peedee belemnite [VPDB] scale). The observed cross-basin trend is largely consistent with cements having formed in response to progressive sediment burial and heating. Within the context of independent burial and thermal history models for the Illinois Basin, cementation began soon after deposition and continued intermittently into the mid-Permian. However, temperatures in excess of burial model predictions are inferred at the time of latest ankerite cement precipitation, which we propose overlapped in time with conductive heating of the Eau Claire Formation (a closed system)

Manuscript received April 6, 2015; provisional acceptance September 28, 2015; revised manuscript received November 19, 2015; final acceptance February 3, 2016.
DOI:10.1306/02031615065

AUTHORS

Maciej G. Śliwiński ~ *WiscSIMS Laboratory, Department of Geoscience, University of Wisconsin–Madison, 1215 W. Dayton St., Madison, Wisconsin 53706; msliwinski@wisc.edu*

Maciej G. Śliwiński received a B.S. in geology from the University of Washington and a Ph.D. in geology from the University of Alaska Fairbanks. He joined the WiscSIMS Laboratory at the University of Wisconsin–Madison as a postdoctoral fellow in 2013. His research interests are chemical and isotopic microanalysis, analytical methods development, x-ray spectroscopy (wavelength-dispersive–x-ray fluorescence, handheld–x-ray fluorescence, and synchrotron-based methods), chemostratigraphy, and sediment diagenesis.

Reinhard Kozdon ~ *WiscSIMS Laboratory, Department of Geoscience, University of Wisconsin–Madison, 1215 W. Dayton St., Madison, Wisconsin 53706; present address: Lamont-Doherty Earth Observatory, Columbia University, 61 Route 9W–PO Box 1000, Palisades, New York 10964; rkozdon@ldeo.columbia.edu*

Reinhard Kozdon received his Ph.D. from the University of Kiel in geology. He was a research scientist at the WiscSIMS Laboratory, University of Wisconsin–Madison, from 2007 to 2014, and he is presently an assistant research professor at the Lamont-Doherty Earth Observatory of Columbia University. His current research applies in situ measurements of stable isotopes and minor elements in foraminiferal shells by secondary ion mass spectrometry and electron probe microanalysis.

Kouki Kitajima ~ *WiscSIMS Laboratory, Department of Geoscience, University of Wisconsin–Madison, 1215 W. Dayton St., Madison, Wisconsin 53706; saburo@geology.wisc.edu*

Kouki Kitajima received his M.S. degree and Ph.D. from Tokyo Institute of Technology, Japan, in geology. He was awarded a postdoctoral fellowship from the Japan Society for the Promotion of Science at the University of Tokyo in 2007 and joined WiscSIMS Laboratory at the University of Wisconsin–Madison in 2010. His

research is focused on in situ stable isotope geochemistry (C, O, and S) of igneous and sedimentary rocks by secondary ion mass spectrometry.

ADAM DENNY ~ *WiscSIMS Laboratory, Department of Geoscience, University of Wisconsin–Madison, 1215 W. Dayton St., Madison, Wisconsin 53706; adam.c.denny@gmail.com*

Adam Denny received his B.A. in geology from Carleton College, and he is currently an M.S. student at the University of Wisconsin–Madison. He is studying carbon and oxygen isotopic variability in diagenetic carbonates in sandstones using secondary ion mass spectrometry.

JOHN W. VALLEY ~ *WiscSIMS Laboratory, Department of Geoscience, University of Wisconsin–Madison, 1215 W. Dayton St., Madison, Wisconsin 53706; valley@geology.wisc.edu*

John Valley received his A.B. from Dartmouth College and his Ph.D. from the University of Michigan in geology. He has been at the University of Wisconsin–Madison since 1983, has served as department chair, is a past president of the Mineralogical Society of America, and is presently the Charles R. Van Hise Distinguished Professor. His current research applies bulk and in situ isotope analysis to sedimentary, igneous, and metamorphic rocks from Holocene to Hadean in age, on Earth and elsewhere.

ACKNOWLEDGMENTS

This material is based primarily upon work supported by the US Department of Energy Office of Science, Office of Basic Energy Sciences, Chemical Sciences, Geosciences, and Biosciences Division under award number DE-FG02-93ER14389. The WiscSIMS Laboratory is partly supported by the US National Science Foundation (EAR-1355590). We thank our colleagues at the University of Wisconsin–Madison: N. Kita and J. Kern, for providing secondary ion mass spectrometry support; M. Spicuzza, for calibrating standards for stable isotope ratios; J. Fournelle and P. Gopon, for assistance with scanning electron microscopy/electron probe microanalysis; A. Pollington, A. Hyodo, and

from under- and overlying sandstone aquifers that channeled the flow of hot, Mississippi Valley–type mineralizing brines during the mid-Permian (ca. 270 Ma).

INTRODUCTION

Studies of sandstone–shale diagenesis commonly employ the oxygen isotope ($\delta^{18}O$) ratios of zoned carbonate mineral cements to constrain (1) temperatures during sediment burial and cementation, (2) the evolution of pore fluid $\delta^{18}O$, (3) the pathways and timing of fluid or brine migration events, and (4) the sources of cementing material (e.g., Arthur et al., 1983; Dutton and Land, 1985; Longstaffe, 1989; Chen, 2001; Fayek et al., 2001; Pollington et al., 2011; Hyodo et al., 2014). The fractionation of oxygen isotopes that occurs between the pore fluid and the carbonate mineral phase during precipitation is large at near-surface conditions and decreases appreciably with increasing temperature throughout the realm of diagenesis (surface to ~300°C [550°F]; Milliken, 2003). The $\delta^{18}O$ values that are preserved in zoned cements can thus serve as a proxy record of sediment burial temperatures, provided that pore fluid $\delta^{18}O$ values in the sedimentary system in question can be reasonably constrained.

Recent advances in the methods of carbon and $\delta^{18}O$ analysis from carbonate minerals by secondary ion mass spectrometry (SIMS) afford the ability to investigate isotopic records in situ with a spatial resolution of mere micrometers (Valley and Kita, 2009; Śliwiński et al., 2015a, b). The ability to make such measurements in situ from a grain mount or a thin section allows, for example, for resolving compositional differences in finely zoned cements and for directly correlating distinct isotopic signatures of different cement generations to petrographic textures (e.g., Śliwiński et al., 2015c). Many of the signal-averaging effects inherent to the microdrilling techniques widely employed in sampling for conventional isotope analysis can be thus circumvented, all the while providing results with a comparable level of both analytical accuracy and precision.

This work documents systematic, burial-depth–related changes in the mineralogy and $\delta^{18}O$ values of successive generations of zoned dolomite–ankerite cements within shaly sandstone beds of the predominantly silty–shaly Upper Cambrian Eau Claire Formation of the Illinois Basin (United States) (Figure 1). We focus specifically on first-order trends in the evolution of carbonate cement $\delta^{18}O$ values, and we evaluate them in relation to the thermal history of lower Paleozoic sedimentary sequences within the basin via $\delta^{18}O$-based modeling of cement precipitation temperatures. These strata were affected not only by heating resulting from progressive burial during the largely continuous episode of basin subsidence from the Late Cambrian to the

mid-Permian but also by a hydrothermal event, dated to circa 270 Ma (mid-Permian), that resulted in the formation of regional Mississippi Valley–type (MVT) ore deposits (lead–zinc mineralization). We integrate our findings with independent burial and thermal history reconstructions for the Illinois Basin (Rowan et al., 2002; Makowitz et al., 2006) to thus constrain the timing of carbonate cementation.

The Eau Claire Formation serves as the primary reservoir seal rock at the Illinois Basin Decatur Project (IBDP), a demonstration site for the feasibility of long-term carbon capture and storage in saline sandstone reservoirs (e.g., Leetaru et al., 2009; US Department of Energy, 2010; Leetaru and Freiburg, 2014). Among the anticipated outcomes of carbon dioxide (CO_2) injection is the eventual precipitation of iron–magnesium–calcium (Fe–Mg–Ca) carbonate mineral cements resulting from reactions between CO_2-charged brine and the reservoir and reservoir seal rocks (e.g., Finley, 2005; Liu et al., 2011; Carroll et al., 2013; see also review of Bickle et al., 2013). We therefore discuss the potential applicability of carbonate mineral analysis by the SIMS technique in future monitoring studies at prospective sequestration sites.

BACKGROUND

Eau Claire Formation Lithofacies

The Upper Cambrian Eau Claire Formation is a lithologically heterogeneous unit comprised predominantly of variably silty–sandy shales, with a considerable abundance of interbedded sandstones, siltstones, and carbonates (e.g., Willman et al., 1975; Aswasereelert, 2005; Aswasereelert et al., 2008; Neufelder et al., 2012; Lahann et al., 2014; Palkovic, 2015). The spatial distribution of lithofacies is complex, and considerable lithologic variability has been observed within individual wells on a scale ranging from millimeters to meters; nevertheless, the predominance of silty–sandy shale beds imparts a largely aquitard-like character to this unit (Neufelder et al., 2012; Lahann et al., 2014). Within the study area of central to northern Illinois and southern Wisconsin (Figure 1A, B), the Eau Claire Formation conformably overlies the Mt. Simon Sandstone and is overlain by the Galesville and Ironton Sandstones (Figure 1C).

Relatively few wells exist wherein the Eau Claire Formation interval was cored (either partially or wholly), thus hindering a thorough characterization of the internal stratigraphy and limiting lateral correlations of specific lithofacies across the Illinois Basin (Neufelder et al., 2012; Lahann et al., 2014). Borehole wireline logs (gamma ray, sonic, neutron, etc.) constitute the most widely available source of subsurface information on this unit. Lahann et al. (2014) thus interpreted rock types from well log data

W. Aswasereelert for access to existing samples; and B. Hess, for help with sample preparation. For assistance with sampling, we thank the staff of the Illinois State Geological Survey and of the Wisconsin Geological and Natural History Survey. We are grateful to A. Makowitz and R. Lander for constructive input regarding the burial history of the Eau Claire Formation.

Datashare 71

Tables A.1 and A.2, Figure A.1, Plates 1–5, and Appendices 1–5 are available in an electronic version on the AAPG website (www.aapg.org/datashare) as Datashare 71.

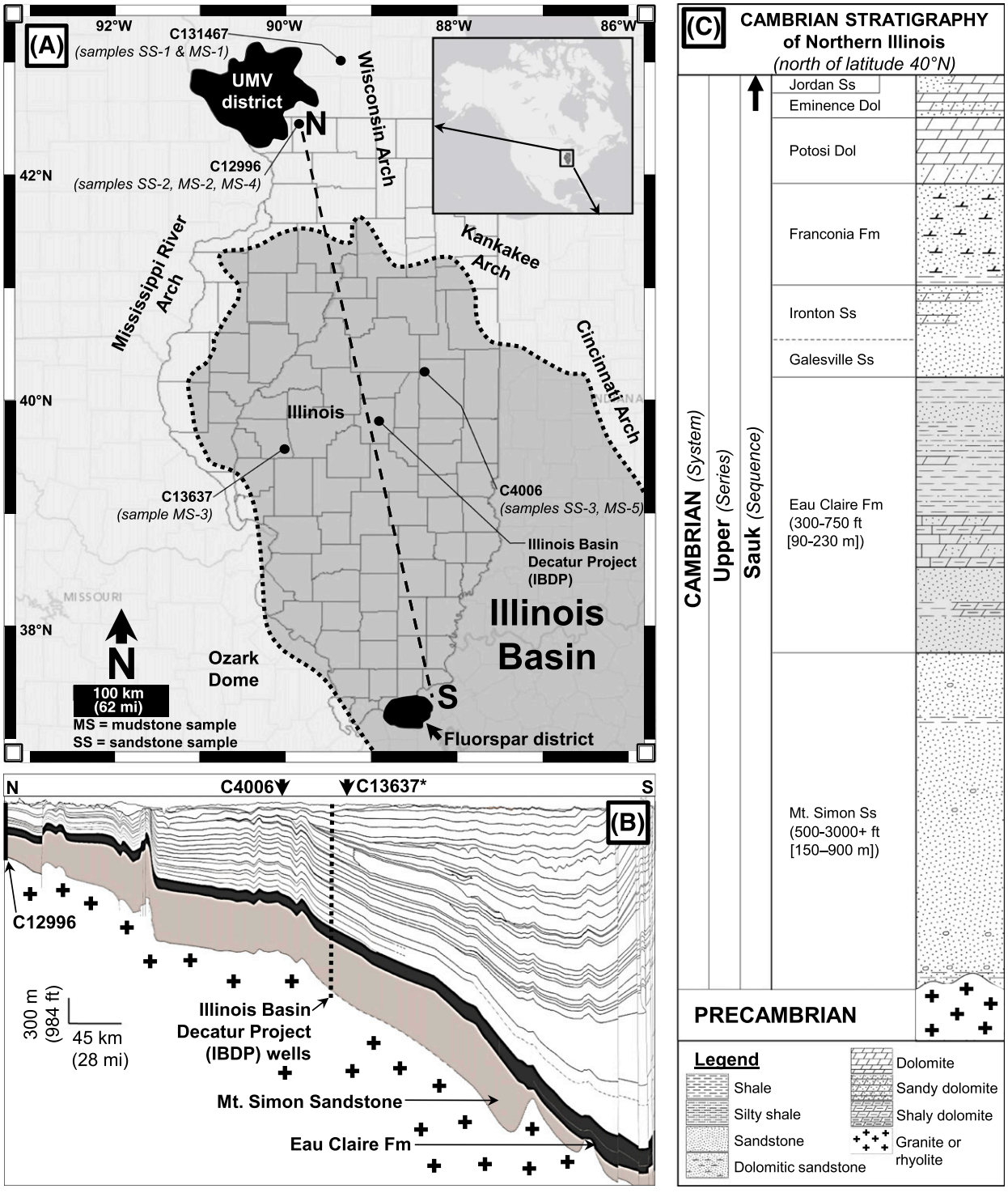

Figure 1. (A) Locations of drill holes sampled for this study of the Eau Claire Formation (Fm) (location of structural arches, domes, and geographic extent of Illinois Basin after Kolata and Nelson, 2010; geographic extent of Upper Mississippi Valley (UMV) and Fluorspar districts after Rowan et al., 2002). (B) North–south (NS) cross section of the Illinois Basin along line NS (in A) showing the Mt. Simon reservoir sandstone draping pre-Cambrian crystalline basement (+ symbols), with the overlying Eau Claire Fm acting as a reservoir seal. Modified after Kolata (2005). Note that Core C13637 is situated to the west of cross section line NS, nearer the basin margin, and thus the Eau Claire Fm is encountered at somewhat shallower depths (see Table 1) than in the projection onto the line NS. (C) Cambrian stratigraphy of the Illinois Basin, north of 40° north latitude. Modified after Kolata (2005). Dol = dolomite; Ss = sandstone.

by means of a statistical clustering procedure that was calibrated with core material where available; a total of 12 distinct lithofacies were identified, which can be reduced to the following 7 on the basis of relatively similar petrophysical properties: (1) sand–silt, (2) muddy sand–silt, (3) silty–sandy shale, (4) muddy shale, (5) dolomitic shale, (6) muddy dolomite, and (7) limestone or dolostone. Based on apparent patterns in the regional distribution of these lithofacies, the Eau Claire Formation can be subdivided into three dominant units. The base of the lowermost unit 1 consists predominantly of silt–sand and muddy silt–sand, which is overlain by an interval of mixed lithologies dominated by dolomitic shale and silty–sandy shale. The middle unit 2 consists predominantly of silty–sandy shale. The topmost unit 3 consists predominantly of dolomite or dolomitic shale. Unit 3 represents much of the Eau Claire section at the southern end of the Illinois Basin and thins to the north.

In an assessment of undiscovered oil and gas resources of the Illinois Basin, the US Geological Survey identified five distinct groups of petroleum source rocks, most of which are thought to have generated thermogenic oil and gas; the Eau Claire Formation is one of these five groups, and it may have supplied hydrocarbons to Precambrian through Ordovician strata, although no quantitative evaluation has been carried out to date (Swezey, 2007, 2009).

Burial and Thermal History of the Illinois Basin

The Illinois Basin originated as a result of rifting on the southern margin of the North American craton during the latest pre-Cambrian, in association with the breakup of the supercontinent Rodinia (e.g., Nelson, 1991). By the Late Cambrian, the basin had evolved into a slowly subsiding cratonic embayment where shallow marine sedimentation of clastic and carbonate strata predominated until the Late Pennsylvanian (e.g., Willman et al., 1975). The basal Mt. Simon Sandstone (Cambrian), which drapes crystalline basement rocks, was buried by the late Permian to maximum depths of approximately 2–2.5 km (~6500–8000 ft) in northern and central Illinois, with temperatures resulting from burial not exceeding approximately 100°C (~200°F) (Fishman, 1997; Makowitz et al., 2006). Uplift in response to the formation of the Ouachita orogenic belt during the late Paleozoic subsequently resulted in a gradual, long-term cooling trend toward present-day temperatures (e.g., ~45°C–50°C [~115°F–120°F] at the IBDP site in central Illinois at depths of 1500–2000 m [4900–6500 ft]; Labotka et al., 2015). We employed data from Makowitz (2004) to plot a simple burial history for the Eau Claire Formation (Figure 2), using tabulated parameters for the top of the underlying Mt. Simon Sandstone as a representation of the base of the Eau Claire.

Hydrothermal heating during the mid-Permian was likely a significant component in the thermal evolution of sedimentary strata in the Illinois Basin. For example, cross-basin trends in the anomalously high thermal maturity of Pennsylvanian coals and trends in paleotemperature measurements from fluid inclusions in mid-Permian MVT ore deposits situated on the basin's southern (~135°C–175°C [~275°F–350°F]) and northern (~100°C–150°C [~215°F–300°F]) margins (Figure 1A) are indicative of a transient heating event during which temperatures exceeded burial model predictions that assume an average geothermal gradient of approximately 30°C/km (1.6°F/100 ft) (reviewed by Rowan et al., 2002). Further, an analysis of fluid inclusions contained within quartz overgrowths in the Mt. Simon Sandstone indicates that this basal sedimentary unit was subjected to a thermal regime where temperatures reached at least as high as ~140°C (~285°F) in the southern regions of the basin and ~120°C (~250°F) on the basin margin in northern Illinois

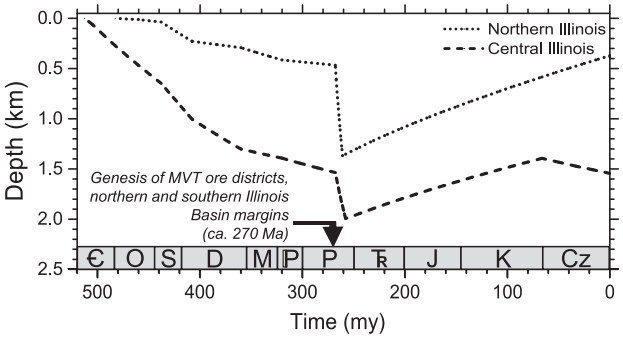

Figure 2. Burial history of the Eau Claire Formation (after Makowitz, 2004, using as a datum the top of the Mount Simon Sandstone) (2.5 km ≈ 8000 ft). C = Cambrian; Cz = Cenozoic; D = Devonian; J = Jurassic; K = Cretaceous; M = Mississippian; MVT = Mississippi Valley–type; O = Ordovician; P (1) = Pennsylvanian; P (2) = Permian; S = Silurian; T_R = Triassic.

(Chen 2001), whereas temperatures no higher than approximately 100°C (~210°F) have been inferred from burial alone (Fishman, 1997; Makowitz et al., 2006).

Rowan et al. (2002) evaluated several end-member scenarios to help constrain the burial and thermal history of the Illinois Basin. In an attempt to satisfy the temperature constraints imposed by MVT ore-hosted fluid inclusions and the cross-basin trends in Pennsylvanian coal maturities, these end-member models considered the effects of (1) additional heat supplied only by deeper burial under a wedge of super-Pennsylvanian sediments (thickening north–south from 0.7 to 1.2 km [~2300 to 3900 ft]) that has since been uplifted and eroded, (2) additional heat supplied by a brief episode (~2 m.y. in duration) of mid-Permian magmatic activity at depth in the southern Illinois basin region (e.g., Zartman, 1977; Moorehead, 2013), and (3) additional heat supplied by magmatic activity as in the second scenario above and its redistribution across the basin by a concurrently active topographically driven fluid-flow system. It was concluded that this third scenario most adequately recreates geological observations and geochemical constraints. Magmatic heat could have been effectively advected northward across the basin by topographically driven fluid flow, channeled through lower Paleozoic sandstone aquifers (e.g., Bethke, 1985, 1986, 1989; Sverjensky, 1986; Bethke and Marshak, 1990). In such a scenario, regional fluid flow would have likely been recharged in the highlands of the Ouachita fold and the thrust belt to the south, and it would have been active until the basin was structurally isolated from the recharge zone by the uplift of the Pascola arch (250–100 Ma; cf., Rowan et al., 2002; Kolata and Nelson, 2010).

OVERVIEW OF THE ANALYTICAL METHODOLOGY

We provide here only a brief overview of the analytical methodology; a more in-depth description can be found in Appendix 1, supplementary material available as AAPG Datashare 71 at www.aapg.org/datashare.

The shaly sandstone beds examined in this study were collected from the basal unit of the predominantly silty–shaly Eau Claire Formation (unit 1; cf., Lahann et al., 2014) at three cored localities (Figure 1A, B; Table 1) that represent different maximum burial depths: (1) the Wisconsin arch (sample SS-1, <0.5 km [<1500 ft]), (2) the basin margin in northern Illinois (sample SS-2, ~1 km [~3500 ft]), and (3) deep burial in central Illinois (sample SS-3, ~2 km [6500 ft]). In terms of the internal lithostratigraphy of this basal Eau Claire unit, the sampled horizons lie above the lowermost low permeability siltstone–shale beds (abbreviated core descriptions can be found in Appendix 2, supplementary material available as AAPG Datashare 71 at www.aapg.org/datashare). Multiple samples were collected from each site and surveyed petrographically by means of backscattered electron (BSE) and cathodoluminescence (CL) scanning electron microscopy (SEM) to locate carbonate-cemented intervals and to identify characteristic stages of the cementation history (Appendix 3, Plates 1–5, supplementary material available as AAPG Datashare 71 at www.aapg.org/datashare). A representative sample from each locality was then chosen for in situ carbonate O-isotope analysis by SIMS. Within each sample, each unique generation of carbonate cement was analyzed repeatedly to ensure that measured $\delta^{18}O$ values are indeed representative. Samples were prepared into 25-mm (1-in.)-diameter epoxy mounts and polished to a 0.25-μm finish using oil-based polycrystalline diamond suspensions. A thin carbon coat (25 nm) was applied to make sample surfaces electrically conductive for imaging by SEM and for analysis by SIMS and electron probe microanalysis (EPMA).

Select Eau Claire Formation shale beds were sampled near each of the sampled shaly sandstone horizons (Figure 1A; Table 1) and submitted to ActLabs (Ancaster, Ontario, Canada) for bulk mineralogical and clay mineral speciation analyses. The abundance of illite and smectite in clay mineral separates was assessed using Środoń's (1984) intensity ratio (IR).

In situ $\delta^{18}O$ measurements (3- and 10-μm-diameter analysis spot size) were performed using a CAMECA IMS 1280 large radius multicollector ion microprobe at the Wisconsin Secondary Ion Mass Spectrometer Laboratory (WiscSIMS; Department of Geoscience, University of Wisconsin–Madison). Measured isotope ratios are reported as per mil deviations relative to the Vienna standard mean ocean water (VSMOW) and Vienna Peedee

Table 1. Bulk Mineralogy and Clay Speciation of Select Eau Claire Formation Shale Samples

Shale Sample	Equivalent Shaly Sandstone Sample (See Table 3)	Core Identification	Present Depth (ft)	Present Depth (m)	Maximum Burial Depth[¶] (ft)	Maximum Burial Depth[¶] (km)	Mineral Mineralogy (vol. %; Bulk Powder XRD Analysis) Quartz	K-feldspar	Muscovite (includes illites)	Chlorite	Dolomite	Ankerite	Pyrite	Amorphous	Clay Mineralogy of the Sub-2 μm Fraction (vol. %) Illite	Chlorite	IR[#]
MS-1	SS-1*	C131467*	294.5	89.8	<1500	<0.5	n.d.	63.5	9.2	n.d.	19.8	n.d.	2.2	5.3	100	n.d.	1
MS-4	SS-2[†]	C12996[†]	1016.7	309.9	~3500	~1 km	8.2	29.8	29.3	2.0	16.3	n.d.	0.5	14.0	96	4	1.16 (<15% smectite)
MS-3	SS-3[§]	C13637[‡]	3597.5	1096.5	~6500	~2 km	12.5	23.9	13.4	3.6	n.d.	17.8	trace	28.8	91	9	1.04 (<15% smectite)
MS-5	SS-3[§]	C4006[§]	3776	1150.9	~6500	~2 km	9.5	15.3	43.2	4.4	n.d.	n.d.	0.7	26.8	96	4	1.39 (<15% smectite)

Refer to Figure 1 regarding core-sampling localities.

Abbreviations: IR = intensity ratio; n.d. = not detected; XRD = x-ray diffraction.

*API number (none), Dane County, Wisconsin (Wisconsin Geological and Natural History Survey).

[†]API number 121772131700, Stephenson County, Illinois (Illinois State Geological Survey).

[‡]API number 121370059800, Morgan County, Illinois (Illinois State Geological Survey).

[§]API number 120190012800, Champaign County, Illinois (Illinois State Geological Survey).

[¶]Present-day burial depth corrected for 0.7 km (~2300 ft) of uplift and erosion in northern and central Illinois and <500 m (<1500 ft) on the Wisconsin arch; see text.

[#]Środoń (1984): IR = $(001/003)_{\text{air dried}}/(001/003)_{\text{glycolated clay mounts}}$. This parameter compares the x-ray intensities of the illite 001 and 003 peaks and is very sensitive to the presence of swelling (smectite) layers. An IR value of 1 indicates that the clay material is 100% nonexpandable, whereas values smaller than ~1.5 are generally consistent with the presence of <15% smectite.

belemnite (VPDB) reference values using conventional delta (δ) notation. The analytical conditions employed were as described in Śliwiński et al. (2015a).

The analytical accuracy of $\delta^{18}O$ measurements by SIMS is affected by instrumental mass fractionation and sample matrix effects (or "bias"; Hervig et al., 1992; Kita et al., 2009; Valley and Kita, 2009), a component of which is systematically related to the chemical composition and crystal structure of a sample. A calibration scheme and suite of standards for correcting SIMS $\delta^{18}O$ bias for carbonate mineral compositions of the dolomite–ankerite solid solution series was reported by Śliwiński et al. (2015a) and employed here for reducing sample data. To implement such corrections, chemical analyses were performed by EPMA in the immediate vicinity of each SIMS pit (using a CAMECA SX-51 at the Cameron Electron Microprobe Laboratory, Department of Geoscience, University of Wisconsin–Madison).

The analytical precision of SIMS analyses is typically ±0.3‰ (two standard deviations [2SD]) for 10-μm-diameter sample spots and ±0.7‰ (2SD) for 3-μm spots, based on the spot-to-spot reproducibility (number of analyses [n] = 8) of running standard analyses that bracket each set of 10 sample analyses. The accuracy of sample analyses is, in part, determined by the calibration residual, which is a measure of how well the SIMS $\delta^{18}O$ bias correction scheme reproduces standard data in relation to the certified reference material NBS-19; for 10-μm spot-size sessions, the residual was constrained to ±0.3‰ (2SD) for a suite of 13 dolomite–ankerite standards, whereas it was within ±0.4‰ (2SD) when performing analyses using a 3-μm spot (Śliwiński et al., 2015a).

RESULTS

Bulk Mineralogy and Clay Speciation of Select Eau Claire Shale Beds

Results of these analyses are presented in Table 1. Noteworthy and significant for the discussion that follows is the fact that illite is the predominant clay type (<15% smectite) in samples from shallow, intermediate, and deep burial alike (Środoń IRs, 1.00–1.39; Środoń, 1984).

Chemical Composition of the Major Carbonate Cement Zones

The petrographic survey of Eau Claire Formation lithofacies reported by Neufelder et al. (2012) indicates that carbonate cements commonly comprise up to approximately 10% of a sample, but in places their volumetric abundance increases to as much as 40%–50%. It was broadly observed that authigenic carbonate is comprised predominantly of (1) early dolomite cement that appears first in the shallow burial environment and (2) late dolomite and ankerite cements that formed during intermediate-deep burial in possible association with hydrocarbon maturation and/or sulfide mineralization.

In our survey of carbonate cements, focused specifically on the sandy intervals of the basal Eau Claire Formation, the predominant cement type encountered in all samples from all depths is represented by compositions that fall along the dolomite–ankerite solid-solution series (Figure 3A; calcite cement was observed only in the shallowest burial environment of the Wisconsin arch). We identified four major, successive stages of dolomite–ankerite cement development (zones 0, 1, 2, and 3) on the basis of discrete changes in chemical composition (Figures 3; 4A, D) and the clustering observed in crossplots of $\delta^{18}O$ versus Fe number (=molar Fe/[Mg + Fe]; Figure 4C, F). These four generations were classified according to the scheme of Chang et al. (1996), which subdivides the dolomite–ankerite solid-solution series into (1) nonferroan dolomite (NFD), characterized by an Fe number between 0.0 and 0.1 (equivalent to 0–5 mol % Fe (i.e., Fe/[Ca + Mg + Fe] × 100); (2) ferroan dolomite (FD), characterized by Fe numbers in the 0.1–0.2 range (equivalent to 5–10 mol % Fe); and (3) ankerite, characterized by Fe numbers greater than 0.2 (equivalent to >10 mol % Fe). In an overarching sense, the chemical composition of the four dolomite–ankerite cement zones evolves with burial depth from NFD to increasingly more Fe-rich ankerite (Figure 3A, B). The cement morphology, however, evolves from sub- to anhedral crystals (<100 μm across) disseminated among sand grains (Figure 5A, C, E) or concentrated in millimeter-scale laminae (Appendix 3, Plate 2 [supplementary material available as AAPG Datashare 71 at www.aapg.org/datashare]) to poikilotopic crystals measuring

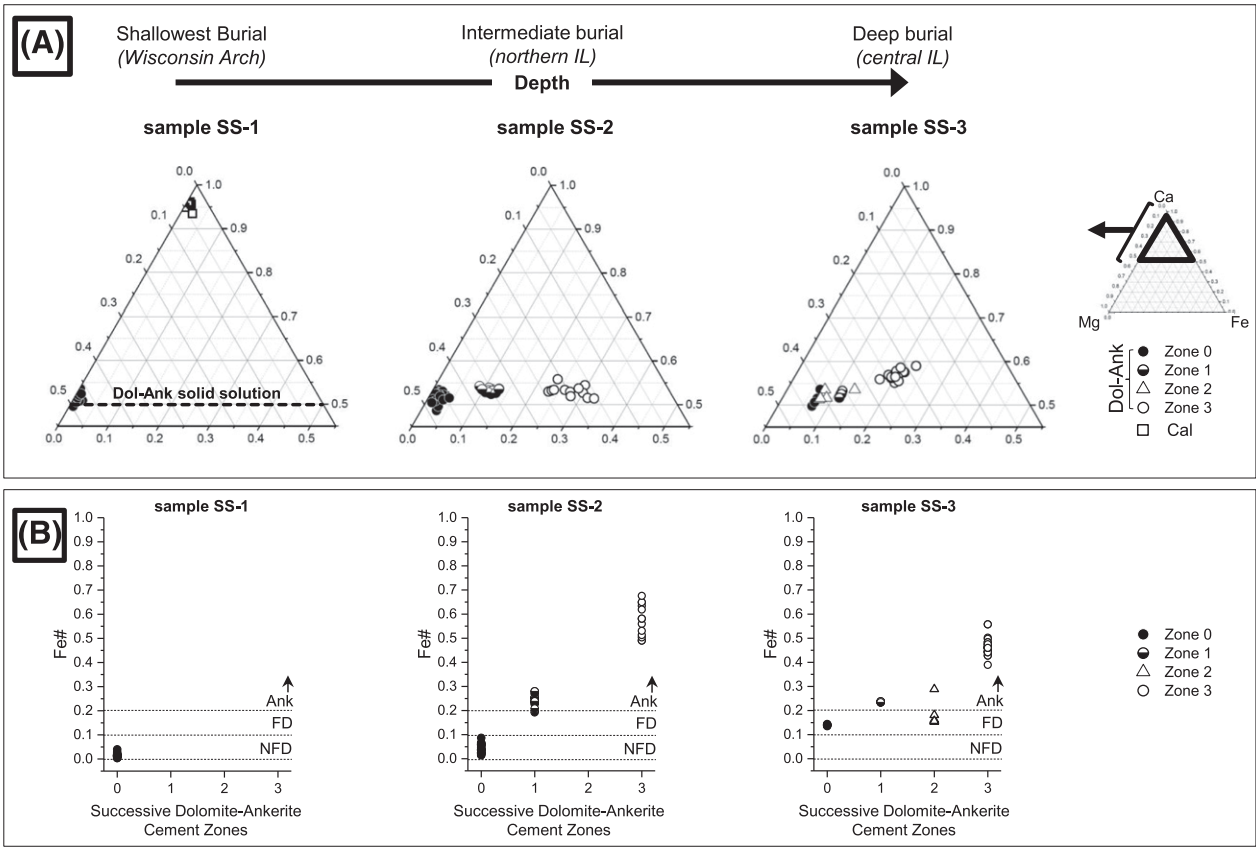

Figure 3. (A) Calcium–magnesium–iron (Ca–Mg–Fe) ternary diagrams depicting the chemical evolution of carbonate cements within shaly sandstone beds of the Eau Claire Formation as a function of increasing paleodepth (sample SS-1 [<0.5 km (~1500 ft)] → SS-2 [~1 km (3500 ft)] → SS-3 [~2 km (6500 ft)]). (B) Compositional zoning evolves from nonferroan dolomite (NFD) to increasingly Fe-rich ankerite (Ank). Sampling localities depicted and detailed in Figure 1 and Table 1. Cal = calcite; Dol = dolomite; FD = ferroan dolomite; IL = Illinois.

up to approximately 500 μm across, with well-developed crystal faces where pore space permits (Figure 4A, D).

Cement zone 0 is present at all three sampled depths and localities. On the Wisconsin arch (sample SS-1; Figure 5A, C, E) and on the basin margin in northern Illinois (SS-2; Figure 4A), it is composed of NFD (Fe number <0.1; Figure 3B). At depth in central Illinois (SS-3; Figure 4D), the composition of zone 0 falls in the FD range of the dolomite–ankerite solid solution (Fe number 0.1–0.2; Figure 3B); imaging by BSE–SEM, which emphasizes relative compositional differences, shows a mottled texture that is suggestive of recrystallization (sensu Machel, 1997; Figure 4D; see also Appendix 3, Plate 5 [supplementary material available as AAPG Datashare 71 at www.aapg.org/datashare]). This mottled texture is not developed in sample SS-2 from shallower burial in northern Illinois (Figure 4A), where BSE–SEM imaging instead reveals fine, micron-scale concentric growth zoning that is readily discernable because of subtle changes in chemical composition (see corresponding CL images in Appendix 3, Plate 1 [supplementary material available as AAPG Datashare 71 at www.aapg.org/datashare]).

Cement zone 1 is absent in the shallowest burial environment of the Wisconsin arch (sample SS-1), but it is present on the basin margin in northern Illinois (SS-2; Figure 4A) and at depth in central Illinois (SS-3; Figure 4D). Compositionally, this zone is a low-Fe ankerite (Fe number 0.2–0.3; Figure 3B) that precipitated on the earlier-formed dolomite cement (zone 0).

Cement zone 2 is present only at depth in central Illinois (sample SS-3), where its development is seen to have followed the sequential growth of zones 0 and 1 (Figure 4D). Zone 2 is predominantly FD (Fe number 0.153–0.182; Figure 3B), although the composition changed abruptly to ankerite (Fe number 0.289; Figure 3B) toward the end of this cement growth phase.

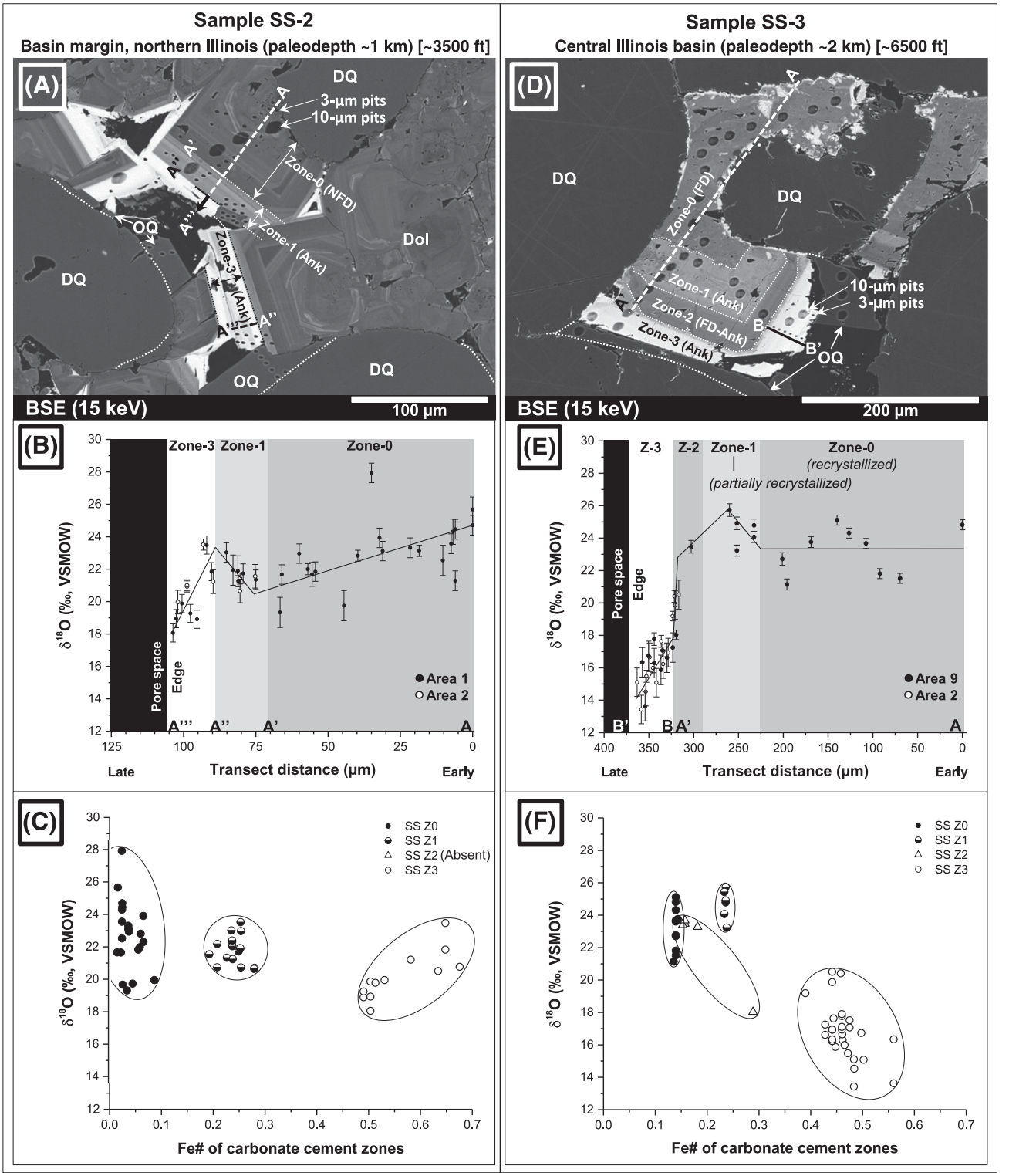
Sample SS-2
Basin margin, northern Illinois (paleodepth ~1 km) [~3500 ft]
(A)
DQ
3-µm pits
10-µm pits
Zone-0 (NFD)
Zone-1 (Ank)
Zone-3 (Ank)
OQ
Dol
DQ
DQ
OQ
A
A'
A''
A'''
BSE (15 keV)
100 µm
(B)
Zone-3
Zone-1
Zone-0
Pore space
Edge
Area 1
Area 2
δ18O (‰, VSMOW)
Transect distance (µm)
Late
Early
(C)
SS Z0
SS Z1
SS Z2 (Absent)
SS Z3
δ18O (‰, VSMOW)
Fe# of carbonate cement zones
Sample SS-3
Central Illinois basin (paleodepth ~2 km) [~6500 ft]
(D)
DQ
Zone-0 (FD)
DQ
Zone-1 (Ank)
Zone-2 (FD-Ank)
Zone-3 (Ank)
10-µm pits
3-µm pits
B
B'
OQ
A
BSE (15 keV)
200 µm
(E)
Z-3
Z-2
Zone-1
Zone-0
(recrystallized)
(partially recrystallized)
Pore space
Edge
Area 9
Area 2
δ18O (‰, VSMOW)
Transect distance (µm)
Late
Early
(F)
SS Z0
SS Z1
SS Z2
SS Z3
δ18O (‰, VSMOW)
Fe# of carbonate cement zones

Cement zone 3 is an ankerite that differs from all preceding carbonate cement generations by its distinctly higher Fe content. It is present on the basin margin in northern Illinois (sample SS-2; Figure 4A) and at depth in central Illinois (SS-3; Figure 4D), having a similar composition at both sampled localities (SS-2: Fe number = 0.569 ± 0.136 [2SD]; SS-3: Fe number = 0.464 ± 0.070 [2SD]; Figure 3B). Its development is seen to have followed the sequential growth of zones 0, 1, and 2 at depth in central Illinois (sample SS-3; Figure 4D), whereas on the basin margin, zone 3 is superimposed directly onto zone 1 (zone 2 is absent).

In a qualitative sense, dolomite cement zone 0 is several times as abundant on the basin margin (sample SS-2) as either zones 1 or 3, which in turn are volumetrically subequal (Figure 4A). The case is similar in central Illinois, where zone 0 is several times as abundant as any of the subsequently formed cement zones 1, 2, or 3, which are approximately subequal in volume (Figure 4D). Cement zones 1 and 3, common to both sampled localities, are approximately twice as thick in central Illinois (SS-3) as they are on the basin margin (SS-2).

Oxygen-Isotope Composition of the Major Carbonate Cement Zones

The results of in situ SIMS $\delta^{18}O$ analyses are summarized in Tables 2 and 3, whereas the complete data sets are provided in Appendices 4 and 5 (supplementary material available as AAPG Datashare 71 at www.aapg.org/datashare); the latter include (1) all measured signals (e.g., count rates, backgrounds, counting statistical errors, etc.) for standards as well as for analyzed sample regions and (2) the calibration model parameters used to correct for SIMS sample matrix effects. Individually annotated SIMS pits, along with supporting petrographic images, are provided in Appendix 3 (supplementary material available as AAPG Datashare 71 at www.aapg.org/datashare).

Cement Zone 0 (Wisconsin Arch, Sample SS-1)

Imaging of this NFD cement by means of CL reveals generally vague, mottled zoning, although in places it is possible to discern that an episode of "CL-dim" dolomite growth likely preceded the formation of "CL-light" regions (Figure 5E, F; Appendix 3, Plate 2E, F [supplementary material available as AAPG Datashare 71 at www.aapg.org/datashare]). The distinctly different $\delta^{18}O$ values of these two different CL domains were only discernable by employing a 3-µm-diameter SIMS beam; the CL-dim domains yielded an average of $\delta^{18}O = 20.3 \pm 1.1$‰ (VSMOW; 2SD, $n = 4$), whereas the subsequently formed CL-light domains yielded a distinctly higher average of 25.6 ± 2.2‰ (2SD, $n = 4$; Figure 5B, E). A larger population of 10-µm spot-size measurements ($n = 22$) yielded a range of $\delta^{18}O$ values between 20.0‰ and 27.0‰, which reflects variable averaging of both the CL-light and CL-dim domains (average = 23.8‰; Figure 5B; Appendix 3, Plate 2E, F [supplementary material available as AAPG Datashare 71 at www.aapg.org/datashare]). A composite $\delta^{18}O$ transect measured from core rim across a larger, planar dolomite crystal (~100 µm across; sensu Sibley and Gregg,

Figure 4. (A) An example of chemo-isotopic zoning in dolomite–ankerite (Dol-Ank) cements within shaly sandstone beds of the Eau Claire Formation on the basin margin in northern Illinois (sample SS-2, paleodepth: ~1 km [3500 ft]). Backscattered electron (BSE) image; refer to Appendix 3, Plate 1A for corresponding cathodoluminescence (CL) image (supplementary material available as AAPG Datashare 71 at www.aapg.org/datashare). (B) In situ measurements of $\delta^{18}O$ (by secondary ion mass spectrometry [SIMS]) in transects across 100-µm-scale cement patches in Sample SS-2 (refer to transects in [A]). (C) Cross-plot of $\delta^{18}O$ vs. cation composition (iron [Fe] number, i.e., molar Fe/[Mg + Fe]) for sample SS-2 (refer to [A, B]). (D) An example of chemo-isotopic zoning in Dol-Ank cements within shaly sandstone beds of the Eau Claire Formation at depth in central Illinois (sample SS-3, paleodepth: ~2 km [6500 ft]). BSE image; refer to Appendix 3, Plate 1B for corresponding CL image (supplementary material available as AAPG Datashare 71 at www.aapg.org/datashare). (E) In situ measurements of $\delta^{18}O$ (by SIMS) in transects across 100-µm-scale cement patches in sample SS-3 (refer to transects in [D]). Note that the $\delta^{18}O$ transects depicted in (B, E) each contain data from two different analyzed sample regions ("Areas"; see Appendix 3 [supplementary material available as AAPG Datashare 71 at www.aapg.org/datashare]). (F) Cross-plot of $\delta^{18}O$ vs. cation composition (Fe number, i.e., molar Fe/[Mg + Fe]) for sample SS-3 (refer to [D, E]). All SIMS pits in (A, B) are individually annotated with their respective $\delta^{18}O$ values in Appendix 3, Plates 4A and 5A (supplementary material available as AAPG Datashare 71 at www.aapg.org/datashare), and can be correlated to the chemical composition data in Table 2 via sample pit– and analytical session–specific measurement identification numbers. DQ = detrital quartz; FD = ferroan dolomite; Mg = magnesium; NFD = non-ferroan dolomite; OQ = overgrowth quartz; VSMOW = Vienna standard mean ocean water; Z = zone.

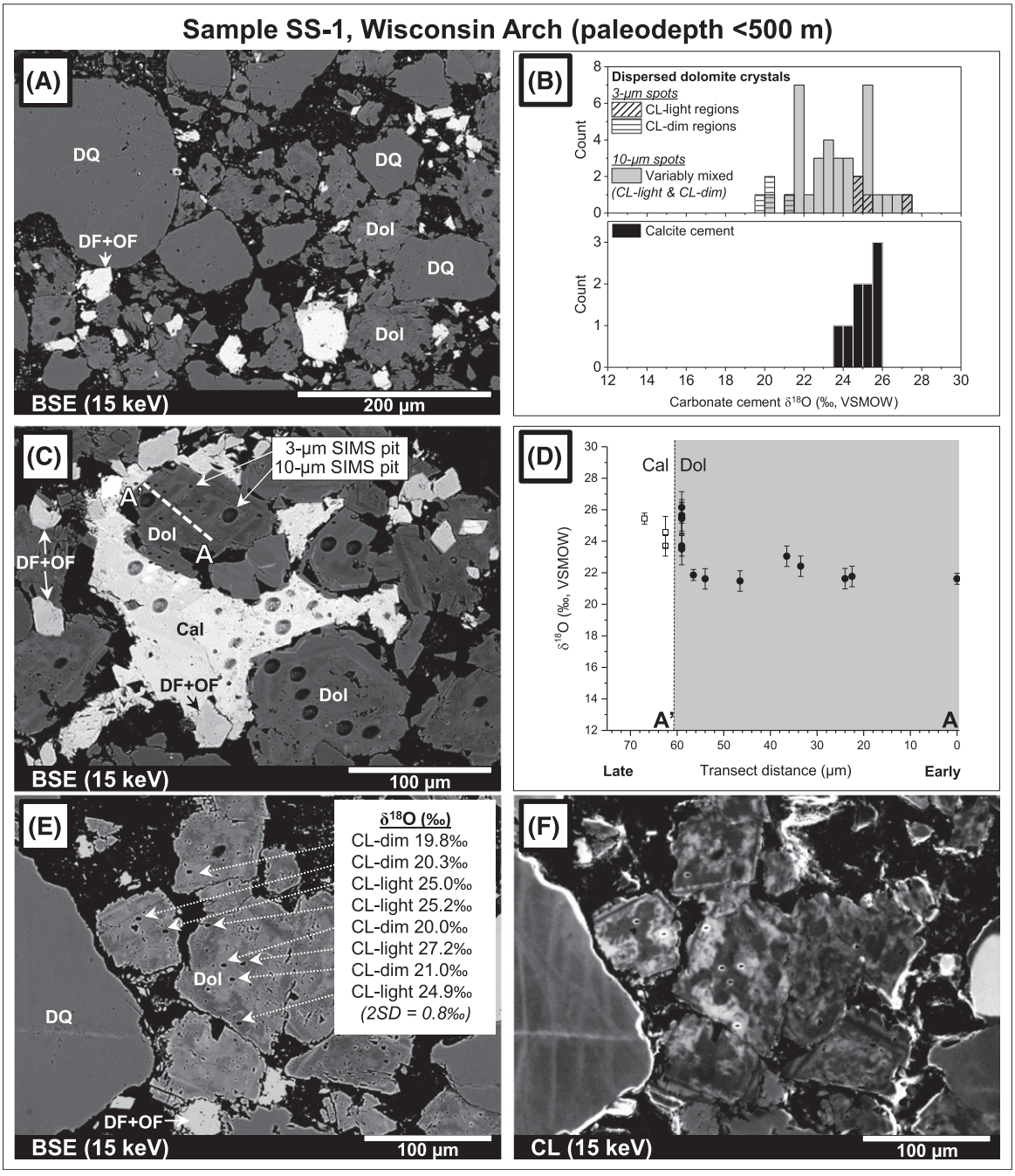

Figure 5. Carbonate cements in the shaly sandstone beds of the Wisconsin arch (sample SS-1; Figure 1, Table 1; maximum paleodepth < 0.5 km [1500 ft]). (A) Anhedral–subhedral dolomite crystals (~30–60 µm across) dispersed among sand grains. Backscattered electron (BSE) image. (B) Measured range of carbonate cement $\delta^{18}O$ values. (C) Larger (~100 µm across) planar dolomite crystals (c.f., Sibley and Gregg, 1987) in contact with patches of calcite cement. BSE image; refer to Appendix 3, Plate 3B for corresponding cathodoluminescence (CL) image (supplementary material available as AAPG Datashare 71 at www.aapg.org/datashare). (D) Composite $\delta^{18}O$ transect measured from core to rim across one of the larger dolomite crystals shown in (C) (line AA′). (E) BSE image of a coalesced mass of anhedral–subhedral dolomite crystals. (F) The same mass of dolomite cement as in (E) but viewed in CL mode. This early cement is comprised of isotopically distinct CL-dim and CL-light domains (refer to [B]). All secondary ion mass spectrometry (SIMS) analysis pits are individually annotated with their respective $\delta^{18}O$ values in Appendix 3, Plates 2 and 3 (supplementary material available as AAPG Datashare 71 at www.aapg.org/datashare), and can be correlated to the chemical composition data in Table 2 via sample pit– and analytical session–specific measurement identification numbers. Cal = calcite; DF = detrital K-feldspar; Dol = dolomite; DQ = detrital quartz; OF = overgrowth K-feldspar; VSMOW = Vienna standard mean ocean water; 2SD = two standard deviations.

1987) shows near-constant values of 21.9 ± 1.1‰ (n = 8), which increase abruptly to a high of 25.0 ± 2.2‰ near the outer rim (Figure 5D). The rims of this and similar crystals show concentric, 1- to 5-µm-scale CL zoning and are in direct contact with calcite cement (Appendix 3, Plate 3 [supplementary material available as AAPG Datashare 71 at www.aapg.org/datashare]). Measured $\delta^{18}O$ (calcite) values average 25.0 ± 1.5‰ (2SD; n = 9; Figure 5B, D; Appendix 3, Plate 3 [supplementary material available as AAPG Datashare 71 at www.aapg.org/datashare]).

Cement Zones 0, 1, and 3 (Basin Margin in Northern Illinois; Sample SS-2)

The O-isotope composition of the earliest identified dolomite crystal cores of zone 0 was only discernable by employing a 3-µm-diameter SIMS beam, yielding an average $\delta^{18}O$ value of 23.8 ± 2.9‰ (2SD; Figure 4A; Appendix 3, Plates 1A; 4B, C [supplementary material available as AAPG Datashare 71 at www.aapg.org/datashare]). Measurements of $\delta^{18}O$ in transects at the 100-µm scale, extending from dolomite crystal cores to ankerite rims, reveal the following trends: $\delta^{18}O$ values generally decrease from approximately 24‰ to approximately 21‰ across zone 0, then increase slightly to 23‰ across zone 1, and lastly systematically decrease to approximately 18‰ across the final ankerite cement zone 3 (Figure 4B). The difference in $\delta^{18}O$ values between early versus late cement generations (i.e., $\Delta^{18}O$ [early–late]) is thus approximately 6‰.

Cement Zones 0, 1, 2, and 3 (Central Illinois; Sample SS-3)

No early dolomite crystal cores, analogous to those of sample SS-2, were identifiable at depth in central Illinois. In contrast to the cements of sample SS-2, none of the cement zones in sample SS-3 show a CL response (compare Appendix 3, Plate 1A, B [supplementary material available as AAPG Datashare 71 at www.aapg.org/datashare]). Imaging of zones 0 and 1 by BSE–SEM, which emphasizes relative compositional differences, reveals mottled textures that are respectively suggestive of extensive (zone 0) and partial (zone 1) recrystallization (sensu Machel, 1997; Figure 4D; see also Appendix 3, Plate 5 [supplementary material available as AAPG Datashare 71 at www.aapg.org/datashare]). Measurements of $\delta^{18}O$ in transects at the 100-µm scale reveal the following trends: $\delta^{18}O$ values oscillate between approximately 21‰ and approximately 25‰ across zone 0, then increase slightly from approximately 24‰ to 26‰ across zone 1, and lastly systematically decrease to approximately 14‰ across zones 2 and 3 (Figure 4D). If we assume a prerecrystallization value of approximately 24‰ for the no longer discernable crystal cores of zone 0 (by way of analogy with sample SS-2), then the difference in $\delta^{18}O$ values between early versus late cement generations (i.e., $\Delta^{18}O$ [early–late]) is approximately 10‰.

DISCUSSION

Significance of Paleodepth-Related Differences in Carbonate Cement $\Delta^{18}O$ (Early–Late)

Measured values of $\delta^{18}O$ from different generations of carbonate cements can be related to temperatures of precipitation using mineral–water equilibrium fractionation factors; we employ those of O'Neil et al. (1969) for calcite and of Horita (2014) for dolomite. To our knowledge, a fractionation factor between water and an ankerite (of some particular composition) has not yet been experimentally calibrated. It thus remains unknown how the Fe content in the dolomite–ankerite solid solution series affects equilibrium relations relative to end-member dolomite. The recent work of Horita (2014) experimentally constrained the dolomite–water equilibrium fractionation factor for the temperature interval between 80°C and 350°C (176°F and 662°F); this calibration extrapolates well to experiments performed at 25°C–40°C (77°F–104°F) (by Vasconcelos et al., 2005; see figure 3 in Horita, 2014) and thus spans the entire temperature range of the diagenetic realm (surface to ~300°C [550°F]; Milliken, 2003). However, neither the isotopic composition of the pore fluid nor its chemistry can, in most cases, be independently determined for different stages of cement precipitation; thus, this remains a matter of speculation in most studies (typically the pore fluid is assumed to be water rather than a brine; see Horita et al., 1993a, b for a discussion concerning the effects of dissolved salts on O-isotope fractionation in solution).

Table 2. Results of Carbonate Cement Analyses by Secondary Ion Mass Spectrometry (in Situ Oxygen-Isotope Measurements) and Electron Probe Microanalysis (in Situ Chemical Analysis)

Sample	Session Specific Sample Identification	SIMS Session	Sample/Spot Identification	Spot Size (μm)	$\delta^{18}O$ (‰) VPDB	$\delta^{18}O$ (‰) VSMOW	2SD	Zone	Mineralogy	Mg (mol %)	Ca (mol %)	Fe (mol %)	Mn (mol %)	Sr (mol %)	Fe Number	Ca Number	Distance* (μm)	Transect† Distance (μm)
SS-1																		
									Calcite									
	20130925@289.asc	S1	SS-1 (A1) A3 Spot 1	10	−5.2	25.6	0.3	–	Cal	3.67%	96.16%	0.16%	<DL	<DL	–	0.963	–	–
	20130925@291.asc	S1	SS-1 (A1) A3 Spot 3	10	−5.0	25.8	0.3	–	Cal	3.67%	96.16%	0.16%	<DL	<DL	–	0.963	–	–
	20130925@297.asc	S1	SS-1 (A1) A7 Spot 1	10	−4.9	25.8	0.3	–	Cal	4.91%	94.88%	0.20%	<DL	<DL	–	0.951	–	–
	20140513@726.asc	S7	SS-1 (A1) A1 Spot 9	10	−5.3	25.4	0.4	–	Cal	3.43%	95.94%	0.63%	<DL	<DL	–	0.965	–	–
	20140513@727.asc	S7	SS-1 (A1) A1 Spot 10	10	−6.7	24.1	0.4	–	Cal	3.43%	95.94%	0.63%	<DL	<DL	–	0.965	–	–
	20140513@728.asc	S7	SS-1 (A1) A1 Spot 11	10	−5.7	25.0	0.4	–	Cal	4.12%	93.49%	2.39%	<DL	<DL	–	0.958	–	–
	20140513@729.asc	S7	SS-1 (A1) A1 Spot 12	10	−5.4	25.4	0.4	–	Cal	4.12%	93.49%	2.39%	<DL	<DL	–	0.958	–	–
	20140722@330.asc	S8	SS-1 (A1) A1 Spot 1	3	−7.0	23.7	0.7	–	Cal	3.24%	95.24%	1.10%	0.42%	<DL	–	0.967	–	–
	20140722@342.asc	S8	SS-1 (A1) A1 Spot 9	3	−6.1	24.6	1.0	–	Cal	3.20%	96.09%	0.62%	0.09%	<DL	–	0.968	–	–
Average					−5.7	25.0	–	–	–	3.75%	95.27%	0.92%	0.06%	0.00%	–	0.962	–	–
2SD					1.5	1.5	–	–	–	1.10%	2.20%	1.77%	0.28%	0.00%	–	0.011	–	–
									Dispersed dolomite crystals									
	20130925@292.asc	S1	SS-1 (A1) A3 Spot 4	10	−7.3	23.4	0.3	Zone 0	NFD	49.13%	50.02%	0.59%	0.26%	<DL	0.012	0.504	–	–
	20130925@293.asc	S1	SS-1 (A1) A3 Spot 5	10	−6.3	24.5	0.3	Zone 0	NFD	49.13%	50.02%	0.59%	0.26%	<DL	0.012	0.504	–	–
	20130925@294.asc	S1	SS-1 (A1) A3 Spot 6	10	−5.5	25.3	0.3	Zone 0	NFD	49.13%	50.02%	0.59%	0.26%	<DL	0.012	0.504	–	–
	20130925@295.asc	S1	SS-1 (A1) A3 Spot 7	10	−5.3	25.5	0.3	Zone 0	NFD	49.13%	50.02%	0.59%	0.26%	<DL	0.012	0.504	–	–
	20130925@308.asc	S1	SS-1 (A1) A1 Spot 2	10	−4.2	26.6	0.4	Zone 0	NFD	47.35%	51.57%	0.48%	0.59%	<DL	0.010	0.521	–	–
	20130925@313.asc	S1	SS-1 (A1) A5 Spot 1	10	−7.0	23.7	0.4	Zone 0	NFD	49.44%	49.19%	0.77%	0.58%	0.02%	0.015	0.499	–	–
	20130925@314.asc	S1	SS-1 (A1) A5 Spot 2	10	−7.5	23.2	0.4	Zone 0	NFD	49.44%	49.19%	0.77%	0.58%	0.02%	0.015	0.499	–	–
	20130925@315.asc	S1	SS-1 (A1) A5 Spot 3	10	−7.3	23.4	0.4	Zone 0	NFD	49.44%	49.19%	0.77%	0.58%	0.02%	0.015	0.499	–	–
	20130925@316.asc	S1	SS-1 (A1) A5 Spot 4	10	−5.4	25.3	0.4	Zone 0	NFD	49.44%	49.19%	0.77%	0.58%	0.02%	0.015	0.499	–	–
	20130925@317.asc	S1	SS-1 (A1) A5 Spot 5	10	−5.6	25.1	0.4	Zone 0	NFD	46.72%	51.99%	0.62%	0.67%	<DL	0.013	0.527	–	–
	20130925@321.asc	S1	SS-1 (A1) A1 Spot 6	10	−5.9	24.8	0.4	Zone 0	NFD	47.35%	51.57%	0.48%	0.59%	<DL	0.010	0.521	–	–
	20140513@719.asc	S7	SS-1 (A1) A3 Spot 2	10	−7.8	22.9	0.4	Zone 0	NFD	48.08%	50.91%	0.87%	0.15%	<DL	0.018	0.514	–	–
	20140513@720.asc	S7	SS-1 (A1) A3 Spot 3	10	−6.4	24.3	0.4	Zone 0	NFD	47.93%	51.27%	0.21%	0.59%	<DL	0.004	0.517	–	–
	20140513@723.asc	S7	SS-1 (A1) A3 Spot 6	10	−9.0	21.6	0.4	Zone 0	NFD	47.15%	50.76%	1.95%	0.14%	<DL	0.040	0.518	–	–
	20140513@724.asc	S7	SS-1 (A1) A3 Spot 7	10	−10.6	20.0	0.4	Zone 0	NFD	47.93%	50.69%	1.39%	<DL	<DL	0.028	0.514	–	–
	20140513@725.asc	S7	SS-1 (A1) A3 Spot 8	10	−8.0	22.7	0.4	Zone 0	NFD	48.04%	50.52%	0.68%	0.77%	<DL	0.014	0.513	–	–
	20140513@734.asc	S7	SS-1 (A1) A5 Spot 1	10	−5.8	25.0	0.3	Zone 0	NFD	46.92%	51.81%	0.64%	0.62%	<DL	0.013	0.525	–	–
	20140513@735.asc	S7	SS-1 (A1) A5 Spot 2	10	−8.0	22.7	0.3	Zone 0	NFD	47.40%	51.42%	0.55%	0.63%	<DL	0.011	0.520	–	–
	20140513@736.asc	S7	SS-1 (A1) A5 Spot 3	10	−6.5	24.2	0.3	Zone 0	NFD	47.88%	51.24%	0.50%	0.39%	<DL	0.010	0.517	–	–
	20140513@737.asc	S7	SS-1 (A1) A5 Spot 4	10	−3.8	27.0	0.3	Zone 0	NFD	47.05%	51.80%	0.73%	0.41%	<DL	0.015	0.524	–	–
	20140513@738.asc	S7	SS-1′ (A1) A5 Spot 5	10	−9.0	21.6	0.3	Zone 0	NFD	47.54%	51.04%	0.66%	0.77%	<DL	0.014	0.518	–	–
	20140513@739.asc	S7	SS-1 (A1) A5 Spot 6	10	−5.7	25.0	0.3	Zone 0	NFD	47.05%	51.80%	0.73%	0.41%	0.01%	0.015	0.524	–	–

(*continued*)

Table 2. Continued

Sample	Session Specific Sample Identification	SIMS Session	Sample/Spot Identification	Spot Size (μm)	$\delta^{18}O$ (‰) VPDB	$\delta^{18}O$ (‰) VSMOW	2SD	Zone	Mineralogy	Mg (mol %)	Ca (mol %)	Fe (mol %)	Mn (mol %)	Sr (mol %)	Fe Number	Ca Number	Distance* (μm)	Transect† Distance (μm)
Average					−6.7	24.0	–	–	–	48.12%	50.69%	0.72%	0.46%	0.00%	0.015	0.513	–	–
2SD					3.4	3.4	–	–	–	1.94%	1.91%	0.70%	0.43%	0.02%	0.014	0.019	–	–
Coalesced mass of dispersed dolomite crystals																		
	CL light outer regions																	
	20140722@318.asc	S8	SS-1 (A1) A5 Spot 1	3	−5.8	24.9	0.80	Zone 0	NFD	46.16%	53.44%	0.20%	0.21%	<DL	0.004	0.537	–	–
	20140722@319.asc	S8	SS-1 (A1) A5 Spot 2	3	−3.6	27.2	0.80	Zone 0	NFD	46.16%	53.44%	0.20%	0.21%	<DL	0.004	0.537	–	–
	20140722@322.asc	S8	SS-1 (A1) A5 Spot 5	3	−5.5	25.2	0.80	Zone 0	NFD	46.16%	53.44%	0.20%	0.21%	<DL	0.004	0.537	–	–
	20140722@324.asc	S8	SS-1 (A1) A5 Spot 7	3	−5.7	25.0	0.80	Zone 0	NFD	46.16%	53.44%	0.20%	0.21%	<DL	0.004	0.537	–	–
Average					−5.2	25.6	–	–	–	46.16%	53.44%	0.20%	0.21%	0.00%	0.004	0.537	–	–
2SD					2.2	2.2	–	–	–	0.00%	0.00%	0.00%	0.00%	0.00%	0.000	0.000	–	–
	CL dim inner regions																	
	20140722@320.asc	S8	SS-1 (A1) A5 Spot 3	3	−9.6	21.0	0.80	Zone 0	NFD	46.59%	52.22%	0.94%	0.24%	0.01%	0.020	0.528	–	–
	20140722@321.asc	S8	SS-1 (A1) A5 Spot 4	3	−10.6	20.0	0.80	Zone 0	NFD	46.59%	52.22%	0.94%	0.24%	0.01%	0.020	0.528	–	–
	20140722@323.asc	S8	SS-1 (A1) A5 Spot 6	3	−10.3	20.3	0.80	Zone 0	NFD	46.59%	52.22%	0.94%	0.24%	0.01%	0.020	0.528	–	–
	20140722@325.asc	S8	SS-1 (A1) A5 Spot 8	3	−10.8	19.8	0.80	Zone 0	NFD	46.59%	52.22%	0.94%	0.24%	0.01%	0.020	0.528	–	–
Average					−10.3	20.3	–	–	–	46.59%	52.22%	0.94%	0.24%	0.01%	0.020	0.528	–	–
2SD					1.1	1.1	–	–	–	0.00%	0.00%	0.00%	0.00%	0.00%	0.000	0.000	–	–
Transect across larger dolomite crystals with CL-zoned rims (in contact with calcite)																		
	20140513@721.asc	S7	SS-1 (A1) A1 Spot 4	10	−9.0	21.6	0.4	Zone 0	NFD	47.52%	51.23%	1.15%	0.09%	<DL	0.024	0.519	0.0	0.0
	20140722@336.asc	S8	SS-1 (A1) A1 Spot 7	3	−8.9	21.8	0.7	Zone 0	NFD	46.88%	51.55%	1.53%	<DL	0.04%	0.032	0.524	22.5	22.5
	20140722@337.asc	S8	SS-1 (A1) A1 Spot 8	3	−9.0	21.6	0.7	Zone 0	NFD	46.03%	52.73%	1.08%	0.17%	<DL	0.023	0.534	24.0	24.0
	20140722@335.asc	S8	SS-1 (A1) A1 Spot 6	3	−8.2	22.4	0.7	Zone 0	NFD	46.14%	51.79%	1.43%	0.64%	<DL	0.030	0.529	33.5	33.5
	20140722@334.asc	S8	SS-1 (A1) A1 Spot 5	3	−7.6	23.1	0.7	Zone 0	NFD	46.25%	52.21%	1.37%	0.18%	<DL	0.029	0.530	36.5	36.5
	20140722@333.asc	S8	SS-1 (A1) A1 Spot 4	3	−9.1	21.5	0.7	Zone 0	NFD	46.61%	51.99%	1.10%	0.30%	<DL	0.023	0.527	46.5	46.5
	20140722@332.asc	S8	SS-1 (A1) A1 Spot 3	3	−9.0	21.6	0.7	Zone 0	NFD	46.79%	51.88%	1.33%	<DL	<DL	0.028	0.526	54.0	54.0
	20140513@722.asc	S7	SS-1 (A1) A1 Spot 5	10	−8.8	21.9	0.4	Zone 0	NFD	47.35%	51.26%	1.11%	0.28%	<DL	0.023	0.520	56.5	56.5
Average					−8.7	21.9	–	–	–	46.70%	51.83%	1.26%	0.21%	0.01%	0.026	0.526	–	–
2SD					1.1	1.1	–	–	–	1.10%	1.00%	0.35%	0.42%	0.03%	0.007	0.010	–	–
Transect areas directly in contact with calcite																		
	20140722@331.asc	S8	SS-1 (A1) A1 Spot 2	3	−7.0	23.7	0.7	Zone 0	NFD	46.80%	51.95%	1.14%	0.12%	<DL	0.024	0.526	59.0	59.0
	20140722@343.asc	S8	SS-1 (A1) A1 Spot 10	3	−5.1	25.7	1.0	Zone 0	NFD	46.54%	52.19%	1.13%	0.14%	<DL	0.024	0.529	59.0	59.0
	20140722@344.asc	S8	SS-1 (A1) A1 Spot 11	3	−4.6	26.2	1.0	Zone 0	NFD	46.54%	52.19%	1.13%	0.14%	<DL	0.024	0.529	59.0	59.0
	20140722@346.asc	S8	SS-1 (A1) A1 Spot 13	3	−5.3	25.4	1.0	Zone 0	NFD	46.58%	51.91%	1.38%	0.12%	<DL	0.029	0.527	59.0	59.0
	20140722@348.asc	S8	SS-1 (A1) A1 Spot 15	3	−5.3	25.5	1.0	Zone 0	NFD	44.74%	52.25%	2.93%	0.08%	<DL	0.061	0.539	59.0	59.0
	20140722@349.asc	S8	SS-1 (A1) A1 Spot 16	3	−7.2	23.5	1.0	Zone 0	NFD	46.34%	52.28%	1.39%	<DL	<DL	0.029	0.530	59.0	59.0
Average					−5.7	25.0	–	–	–	46.26%	52.13%	1.52%	0.10%	0.00%	0.032	0.530	–	–
2SD					2.2	2.2	–	–	–	1.51%	0.32%	1.41%	0.11%	0.00%	0.030	0.009	–	–

(*continued*)

Table 2. Continued

Sample	Session Specific Sample Identification	SIMS Session	Sample/Spot Identification	Spot Size (μm)	$\delta^{18}O$ (‰) VPDB	$\delta^{18}O$ (‰) VSMOW	2SD	Zone	Mineralogy	Mg (mol %)	Ca (mol %)	Fe (mol %)	Mn (mol %)	Sr (mol %)	Fe Number	Ca Number	Distance* (μm)	Transect† Distance (μm)
SS-2																		
						Sample SS-2 composite transect† (Area 1 AA′: 70.5 μm; AA″: 89.5 μm; AA‴: 104 μm; Area 2 transect segments projected onto Area 1 AA‴)												
	Zone 0, dolomite crystal cores																	
	20140722@188.asc	S8	SS-2 A1 Spot 29	3	−9.3	21.3	0.6	Zone 0	NFD	45.38%	53.38%	1.14%	0.09%	<DL	0.025	0.541	6.0	3.0
	20140722@187.asc	S8	SS-2 A1 Spot 28	3	−6.0	24.7	0.6	Zone 0	NFD	45.38%	53.38%	1.14%	0.09%	<DL	0.025	0.541	0.0	3.0
	20140722@189.asc	S8	SS-2 A1 Spot 30	3	−6.3	24.5	0.6	Zone 0	NFD	45.38%	53.38%	1.14%	0.09%	<DL	0.025	0.541	6.0	3.0
	20140722@166.asc	S8	SS-2 A1 Spot 15	3	−5.1	25.7	0.8	Zone 0	NFD	46.04%	53.03%	0.75%	0.15%	0.03%	0.016	0.535	0.0	3.0
	20140224@387.asc	S4	SS-2 A1 Spot 2	3	−6.4	24.3	0.8	Zone 0	NFD	46.36%	52.30%	1.14%	0.19%	<DL	0.024	0.530	6.8	6.8
	20140722@185.asc	S8	SS-2 A1 Spot 26	3	−7.1	23.6	0.6	Zone 0	NFD	46.36%	52.30%	1.14%	0.19%	<DL	0.024	0.530	7.4	7.4
	20140224@400.asc	S4	SS-2 A1 Spot 11	3	−8.1	22.5	0.9	Zone 0	NFD	46.36%	52.30%	1.14%	0.19%	<DL	0.024	0.530	10.3	10.3
Average					−6.9	23.8	–	–	–	45.89%	52.87%	1.08%	0.14%	0.00%	0.023	0.535	–	–
2SD					2.9	2.9	–	–	–	0.99%	1.09%	0.29%	0.10%	0.02%	0.006	0.010	–	–
						Subsequent stages of zone 0 growth												
	20130924@58.asc	S1	SS-2 A1 Spot1	10	−7.5	23.1	0.3	Zone 0	NFD	47.24%	50.69%	1.82%	0.25%	<DL	0.037	0.518	18.5	18.5
	20140722@186.asc	S8	SS-2 A1 Spot 27	3	−7.4	23.3	0.6	Zone 0	NFD	45.23%	52.59%	1.70%	0.48%	<DL	0.036	0.538	21.6	21.6
	20140722@178.asc	S8	SS-2 A1 Spot 23	3	−7.6	23.1	0.6	Zone 0	NFD	45.23%	52.59%	1.70%	0.48%	<DL	0.036	0.538	31.1	31.1
	20140722@180.asc	S8	SS-2 A1 Spot 25	3	−6.8	23.9	0.6	Zone 0	NFD	44.37%	51.84%	3.10%	0.69%	<DL	0.065	0.539	32.2	32.2
	20140722@179.asc	S8	SS-2 A1 Spot 24	3	−2.9	27.9	0.6	Zone 0	NFD	46.81%	51.73%	1.14%	0.32%	<DL	0.024	0.525	35.0	35.0
	20130924@59.asc	S1	SS-2 A1 R1 Spot2	10	−7.8	22.8	0.3	Zone 0	NFD	48.00%	48.35%	3.07%	0.58%	<DL	0.060	0.502	39.7	39.7
	20140224@397.asc	S4	SS-2 A1 R1 Spot 8	3	−10.8	19.8	0.9	Zone 0	NFD	44.76%	52.97%	2.09%	0.18%	<DL	0.045	0.542	44.5	44.5
	20140722@175.asc	S8	SS-2 A1 Spot 20	3	−8.8	21.9	0.6	Zone 0	NFD	44.75%	51.84%	2.63%	0.74%	0.04%	0.056	0.537	54.4	54.4
	20140224@413.asc	S4	SS-2 A1 Spot 2	3	−8.9	21.7	0.7	Zone 0	NFD	47.33%	51.71%	0.71%	0.25%	<DL	0.015	0.522	55.5	55.5
	20130924@61.asc	S1	SS-2 A1 Spot4	10	−8.6	22.0	0.3	Zone 0	NFD	47.21%	49.35%	2.93%	0.50%	<DL	0.058	0.511	57.0	57.0
	20140722@176.asc	S8	SS-2 A1 Spot 21	3	−7.7	23.0	0.6	Zone 0	NFD	45.81%	52.25%	1.77%	0.17%	<DL	0.037	0.533	60.0	60.0
	20140722@177.asc	S8	SS-2 A1 Spot 22	3	−9.0	21.7	0.6	Zone 0	NFD	46.47%	52.40%	1.04%	<DL	0.09%	0.022	0.530	66.0	66.0
	20140224@396.asc	S4	SS-2 A1 Spot 7	3	−11.2	19.3	0.9	Zone 0	NFD	47.35%	50.93%	1.64%	0.09%	<DL	0.033	0.518	66.6	66.6
Average					−7.7	23.0	–	–	–	46.09%	51.97%	1.65%	0.29%	0.01%	0.034	0.530	–	–
2SD					3.9	3.9	–	–	–	2.04%	2.61%	1.51%	0.43%	0.04%	0.030	0.022	–	–
	20140722@172.asc	S8	SS-2 A1 Spot 17	3	−9.3	21.4	0.6	Zone 1	Ank	36.14%	52.37%	10.58%	0.87%	0.03%	0.226	0.592	75.0	75.0
	20140722@173.asc	S8	SS-2 A1 Spot 18	3	−8.9	21.7	0.6	Zone 1	Ank	34.70%	53.21%	11.51%	0.57%	<DL	0.249	0.605	79.4	79.4
	20130924@60.asc	S1	SS-2 A1 Spot3	10	−9.4	21.3	0.3	Zone 1	Ank	35.77%	52.54%	11.15%	0.54%	<DL	0.238	0.595	81.1	81.1
	20140224@399.asc	S4	SS-2 A1 Spot 10	3	−8.7	21.9	0.9	Zone 1	Ank	35.39%	52.19%	11.93%	0.49%	<DL	0.252	0.596	81.2	81.2
	20140224@395.asc	S4	SS-2 A1 Spot 6	3	−8.7	21.9	0.9	Zone 1	Ank	35.39%	52.19%	11.93%	0.49%	<DL	0.252	0.596	82.9	82.9
	20140722@174.asc	S8	SS-2 A1 Spot 19	3	−7.6	23.0	0.6	Zone 1	Ank	35.14%	53.56%	10.80%	0.46%	0.04%	0.235	0.604	85.2	85.2
Average					−8.8	21.9	–	–	–	35.42%	52.68%	11.32%	0.57%	0.01%	0.242	0.598	–	–
2SD					1.3	1.3	–	–	–	1.00%	1.15%	1.14%	0.30%	0.04%	0.021	0.011	–	–

(*continued*)

Table 2. Continued

Sample	Session Specific Sample Identification	SIMS Session	Sample/Spot Identification	Spot Size (μm)	$\delta^{18}O$ (‰) VPDB	$\delta^{18}O$ (‰) VSMOW	2SD	Zone	Mineralogy	Mg (mol %)	Ca (mol %)	Fe (mol %)	Mn (mol %)	Sr (mol %)	Fe Number	Ca Number	Distance* (μm)	Transect† Distance (μm)
Sample SS-2 Area 1 transect segment A″A‴ (SR 2; 18 μm): projected onto composite transect (Area 1) segment A″A‴ (+AA″)																		
	20140722@151.asc	S8	SS-2 A1 Spot 4	3	−8.8	21.9	0.6	Zone 3	Ank	15.87%	53.92%	29.22%	0.96%	0.04%	0.648	0.773	1.0	90.3
	20140722@153.asc	S8	SS-2 A1 Spot 6	3	−7.2	23.5	0.6	Zone 3	Ank	15.87%	53.92%	29.22%	0.96%	0.04%	0.648	0.773	3.1	92.0
	20140722@150.asc	S8	SS-2 A1 Spot 3	3	−11.6	18.9	0.6	Zone 3	Ank	23.89%	52.84%	22.97%	0.30%	<DL	0.490	0.689	7.2	95.3
	20140722@154.asc	S8	SS-2 A1 Spot 7	3	−11.3	19.3	0.6	Zone 3	Ank	23.89%	52.84%	22.97%	0.30%	<DL	0.490	0.689	10.1	97.6
	20140722@149.asc	S8	SS-2 A1 Spot 2	3	−10.7	19.9	0.6	Zone 3	Ank	23.15%	53.08%	23.47%	0.30%	<DL	0.503	0.696	13.7	100.5
	20140722@155.asc	S8	SS-2 A1 Spot 8	3	−11.6	19.0	0.6	Zone 3	Ank	23.15%	53.08%	23.47%	0.30%	<DL	0.503	0.696	16.2	102.6
	20140722@148.asc	S8	SS-2 A1 Spot 1	3	−12.5	18.1	0.6	Zone 3	Ank	23.15%	53.08%	23.47%	0.30%	<DL	0.503	0.696	17.6	103.7
Average					−10.5	20.1	–	–	–	21.28%	53.25%	24.97%	0.49%	0.01%	0.541	0.716	–	–
2SD					3.8	3.8	–	–	–	7.42%	0.94%	5.82%	0.64%	0.04%	0.147	0.078	–	–
Sample SS-2 Area 2 transect segment A′A″ (14.5 μm)†: projected onto composite transect (Area 1) segment A′A″ (+AA′)																		
	20140224@407.asc	S4	SS-2 A2 Spot 3	3	−9.1	21.6	0.7	Zone 1	FD	36.45%	53.49%	8.69%	1.36%	<DL	0.193	0.595	3.6	75.2
	20140224@408.asc	S4	SS-2 A2 Spot 4	3	−9.9	20.7	0.7	Zone 1	Ank	33.27%	53.08%	12.88%	0.77%	<DL	0.279	0.615	7.6	80.5
	20130924@65.asc	S1	SS-2 A2 Spot3	10	−9.2	21.4	0.3	Zone 1	Ank	34.23%	52.20%	12.65%	0.93%	<DL	0.270	0.604	7.6	80.5
Average					−9.4	21.2	–	–	–	34.65%	52.92%	11.41%	1.02%	0.00%	0.247	0.605	–	–
2SD					1.0	1.0	–	–	–	3.27%	1.32%	4.71%	0.61%	0.00%	0.095	0.020	–	–
Sample SS-2 Area 2 transect segment A″A‴ (37.5 μm)†: projected onto composite transect (Area 1) segment A″A‴ (+ AA″)																		
	20140224@409.asc	S4	SS-2 A2 Spot 5	3	−9.4	21.2	0.7	Zone 3	Ank	19.94%	51.44%	27.68%	0.94%	<DL	0.581	0.721	0.7	89.8
	20130924@66.asc	S1	SS-2 A2 Spot 4	10	−7.2	23.5	0.3	Zone 3	Ank	16.85%	51.18%	31.23%	0.74%	<DL	0.650	0.752	9.5	93.2
	20130924@67.asc	S1	SS-2 A2 Spot 5	10	−9.7	20.9	0.3	Zone 3	Ank	19.71%	52.93%	27.30%	0.05%	<DL	0.581	0.729	24.0	98.8
	20130924@68.asc	S1	SS-2 A2 Spot 6	10	−9.6	21.0	0.3	Zone 3	Ank	19.71%	52.93%	27.30%	0.05%	<DL	0.581	0.729	24.0	98.8
	20140224@410.asc	S4	SS-2 A2 Spot 6	3	−10.6	20.0	0.7	Zone 3	Ank	20.58%	55.39%	23.27%	0.75%	<DL	0.531	0.729	32.3	102.0
Average					−9.3	21.3	–	–	–	19.36%	52.77%	27.36%	0.51%	0.00%	0.585	0.732	–	–
2SD					2.6	2.6	–	–	–	2.89%	3.35%	5.64%	0.85%	0.00%	0.085	0.023	–	–
Additional areas analyzed†																		
	20140224@405.asc	S4	SS-2 A2 Spot 1	3	−10.9	19.7	0.7	Zone 0	NFD	48.25%	50.46%	1.25%	0.04%	<DL	0.025	0.511	–	–
	20140224@411.asc	S4	SS-2 A2 Spot 7	3	−8.3	22.3	0.7	Zone 0	NFD	45.49%	50.83%	3.18%	0.51%	<DL	0.065	0.528	–	–
	20140224@406.asc	S4	SS-2 A2 Spot 2	3	−10.6	20.0	0.7	Zone 0	NFD	43.88%	51.09%	4.15%	0.88%	<DL	0.086	0.538	–	–
	20130924@63.asc	S1	SS-2 A2 Spot 1	10	−7.5	23.1	0.3	Zone 0	NFD	47.28%	50.75%	1.76%	0.22%	<DL	0.036	0.518	–	–
	20130924@64.asc	S1	SS-2 A2 Spot 2	10	−7.2	23.5	0.3	Zone 0	NFD	47.63%	51.16%	1.11%	0.10%	<DL	0.023	0.518	–	–
	20140722@207.asc	S8	SS-2 A1 Spot 40	3	−9.9	20.7	0.7	Zone 1	Ank	33.05%	53.11%	12.84%	1.00%	<DL	0.280	0.616	–	–
	20140722@164.asc	S8	SS-2 A1 Spot 13	3	−8.3	22.3	0.8	Zone 1	Ank	35.47%	53.07%	10.99%	0.47%	<DL	0.237	0.599	–	–
	20140722@206.asc	S8	SS-2 A1 Spot 39	3	−8.6	22.1	0.7	Zone 1	Ank	35.47%	53.07%	10.99%	0.47%	<DL	0.237	0.599	–	–
	20140722@208.asc	S8	SS-2 A1 Spot 41	3	−7.1	23.5	0.7	Zone 1	Ank	34.80%	52.84%	11.82%	0.54%	<DL	0.253	0.603	–	–
	20140722@163.asc	S8	SS-2 A1 Spot 12	3	−8.2	22.4	0.8	Zone 1	Ank	35.47%	53.07%	10.99%	0.47%	<DL	0.237	0.599	–	–
	20140722@205.asc	S8	SS-2 A1 Spot 38	3	−7.7	23.0	0.7	Zone 1	Ank	34.80%	52.84%	11.82%	0.54%	<DL	0.254	0.603	–	–
	20140722@204.asc	S8	SS-2 A1 Spot 37	3	−9.9	20.8	0.7	Zone 1	Ank	34.80%	52.84%	11.82%	0.54%	<DL	0.254	0.603	–	–

(*continued*)

Table 2. Continued

Sample	Session Specific Sample Identification	SIMS Session	Sample/Spot Identification	Spot Size (μm)	$\delta^{18}O$ (‰) VPDB	$\delta^{18}O$ (‰) VSMOW	2SD	Zone	Mineralogy	Mg (mol %)	Ca (mol %)	Fe (mol %)	Mn (mol %)	Sr (mol %)	Fe Number	Ca Number	Distance* (μm)	Transect† Distance (μm)
	20140722@190.asc	S8	SS-2 A1 Spot 31	3	−8.5	22.2	0.6	Zone 1	Ank	36.30%	52.71%	9.53%	1.46%	<DL	0.208	0.592	–	–
	20140722@152.asc	S8	SS-2 A1 Spot 5	3	−9.8	20.8	0.6	Zone 1	Ank	36.30%	52.71%	9.53%	1.46%	<DL	0.208	0.592	–	–
	20140224@394.asc	S4	SS-2 A1 Spot 5	3	−10.1	20.5	0.9	Zone 3	Ank	17.29%	52.68%	29.96%	0.06%	<DL	0.634	0.753	–	–
	20140224@388.asc	S4	SS-2 A1 Spot 3	3	−10.8	19.8	0.8	Zone 3	Ank	22.58%	53.15%	23.79%	0.48%	<DL	0.513	0.702	–	–
	20140224@393.asc	S4	SS-2 A1 Spot 4	3	−9.8	20.8	0.9	Zone 3	Ank	15.73%	51.31%	32.77%	0.19%	<DL	0.676	0.765	–	–
SS-3																		
					Composite transect† (Area 9; AA′: 316.6 μm + Area 9 segment BB′ (48.6 μm) and Area 2 segment CC′ (36.7 μm) projected onto BB′).													
	20140513@640.asc	S7	SS-3 A9 Spot 3	10	−5.9	24.8	0.3	Zone 0	FD	42.30%	50.52%	6.86%	0.31%	0.03%	0.140	0.544	0.0	0.0
	20140513@639.asc	S7	SS-3 A9 Spot 2	10	−9.1	21.5	0.3	Zone 0	FD	42.30%	50.52%	6.86%	0.31%	0.03%	0.140	0.544	69.6	69.6
	20140513@642.asc	S7	SS-3 A9 Spot 5	10	−8.8	21.8	0.3	Zone 0	FD	42.30%	50.52%	6.86%	0.31%	0.03%	0.140	0.544	92.1	92.1
	20140513@643.asc	S7	SS-3 A9 Spot 6	10	−7.0	23.7	0.3	Zone 0	FD	42.30%	50.52%	6.86%	0.31%	0.03%	0.140	0.544	107.7	107.7
	20140513@644.asc	S7	SS-3 A9 Spot 7	10	−6.4	24.3	0.3	Zone 0	FD	42.30%	50.52%	6.86%	0.31%	0.03%	0.140	0.544	126.6	126.6
	20140513@645.asc	S7	SS-3 A9 Spot 8	10	−5.6	25.1	0.3	Zone 0	FD	42.30%	50.52%	6.86%	0.31%	0.03%	0.140	0.544	140.0	140.0
	20130925@356.asc	S1	SS-3 A9 Spot 9	10	−6.9	23.8	0.3	Zone 0	FD	41.37%	51.44%	6.93%	0.26%	<DL	0.143	0.554	169.0	169.0
	20130925@355.asc	S1	SS-3 A9 Spot 8	10	−9.5	21.1	0.3	Zone 0	FD	43.22%	49.59%	6.78%	0.36%	0.05%	0.136	0.534	196.0	196.0
	20140513@650.asc	S7	SS-3 A9 Spot 9	10	−8.0	22.7	0.4	Zone 0	FD	42.30%	50.52%	6.86%	0.31%	0.03%	0.140	0.544	201.1	201.1
Average					−7.5	23.2	–	–	–	42.30%	50.52%	6.86%	0.31%	0.03%	0.140	0.544	–	–
2SD					2.9	2.9	–	–	–	0.93%	0.93%	0.08%	0.05%	0.03%	0.004	0.010	–	–
	20140513@653.asc	S7	SS-3 A9 Spot 12	10	−5.9	24.8	0.4	Zone 1	Ank	35.97%	52.02%	11.08%	0.93%	<DL	0.236	0.591	232.6	232.6
	20130925@354.asc	S1	SS-3 A9 Spot 7	10	−6.6	24.1	0.3	Zone 1	Ank	36.60%	51.17%	11.14%	1.09%	<DL	0.233	0.583	232.6	232.6
	20140513@652.asc	S7	SS-3 A9 Spot 11	10	−5.8	24.9	0.4	Zone 1	Ank	35.97%	52.02%	11.08%	0.93%	<DL	0.236	0.591	251.7	251.7
	20130925@353.asc	S1	SS-3 A9 Spot 6	10	−7.4	23.2	0.3	Zone 1	Ank	35.33%	52.88%	11.02%	0.77%	<DL	0.238	0.599	251.7	251.7
	20140513@651.asc	S7	SS-3 A9 Spot 10	10	−5.0	25.7	0.4	Zone 1	Ank	35.97%	52.02%	11.08%	0.93%	<DL	0.236	0.591	260.1	260.1
Average					−6.2	24.5	–	–	–	35.97%	52.02%	11.08%	0.93%	0.00%	0.236	0.591	–	–
2SD					1.9	1.9	–	–	–	0.90%	1.21%	0.08%	0.23%	0.00%	0.003	0.012	–	–
	20140513@656.asc	S7	SS-3 A9 Spot 15	10	−7.2	23.5	0.4	Zone 2	FD	40.58%	51.26%	7.55%	0.61%	<DL	0.157	0.558	302.8	302.8
					Sample SS-3 Area 9 transect segment BB′ (48.6 μm)†: added to composite transect (Area 9) segment AA′													
	20130925@334.asc	S1	SS-3 A2 Spot 1	10	−12.5	18.0	0.3	Zone 2	Ank	32.33%	52.52%	13.12%	2.04%	<DL	0.289	0.619	3.0	319.6
	20140722@378.asc	S8	SS-3 A9 Spot 8	3	−13.2	17.3	0.9	Zone 3	Ank	23.91%	55.21%	17.88%	2.99%	<DL	0.428	0.698	6.8	323.4
	20140722@377.asc	S8	SS-3 A9 Spot 7	3	−13.9	16.6	0.9	Zone 3	Ank	23.91%	55.21%	17.88%	2.99%	<DL	0.428	0.698	13.2	329.8
	20140513@654.asc	S7	SS-3 A9 Spot 13	10	−13.4	17.1	0.4	Zone 3	Ank	22.67%	53.92%	20.51%	2.90%	<DL	0.475	0.704	18.1	334.7
	20140722@376.asc	S8	SS-3 A9 Spot 6	3	−14.6	15.9	0.9	Zone 3	Ank	23.40%	54.62%	18.97%	3.02%	<DL	0.448	0.700	20.0	336.6
	20140513@655.asc	S7	SS-3 A9 Spot 14	10	−12.7	17.8	0.4	Zone 3	Ank	22.87%	55.03%	19.48%	2.62%	<DL	0.460	0.706	27.5	344.1
	20140722@375.asc	S8	SS-3 A9 Spot 5	3	−14.2	16.3	0.9	Zone 3	Ank	22.55%	55.02%	19.33%	3.10%	<DL	0.462	0.709	27.5	344.1
	20140722@374.asc	S8	SS-3 A9 Spot 4	3	−13.8	16.7	0.9	Zone 3	Ank	20.53%	55.75%	20.33%	3.37%	0.03%	0.498	0.731	33.9	350.5
	20140722@371.asc	S8	SS-3 A9 Spot 1	3	−16.8	13.6	0.9	Zone 3	Ank	17.63%	57.35%	22.22%	2.80%	<DL	0.560	0.766	37.7	354.3
	20140722@373.asc	S8	SS-3 A9 Spot 3	3	−14.1	16.3	0.9	Zone 3	Ank	17.63%	57.35%	22.22%	2.80%	<DL	0.560	0.766	40.7	357.3

(*continued*)

Table 2. Continued

Sample	Session Specific Sample Identification	SIMS Session	Sample/Spot Identification	Spot Size (μm)	$\delta^{18}O$ (‰) VPDB	$\delta^{18}O$ (‰) VSMOW	2SD	Zone	Mineralogy	Mg (mol %)	Ca (mol %)	Fe (mol %)	Mn (mol %)	Sr (mol %)	Fe Number	Ca Number	Distance* (μm)	Transect† Distance (μm)
Average					−14.1	16.4	–	–	–	21.68%	55.50%	19.87%	2.95%	0.00%	0.480	0.720	–	–
2SD					2.4	2.4	–	–	–	5.01%	2.32%	3.23%	0.43%	0.02%	0.101	0.056	–	–
Sample SS-3 Area 2 transect segment CC′ (36.7 μm)†: projected onto composite transect (Area 9) segment BB′ and added to AA′																		
	20140722@365.asc	S8	SS-3 A2 Spot 8	3	−15.3	15.1	0.9	Zone 3	Ank	20.67%	56.66%	19.33%	3.34%	<DL	0.483	0.733	1.5	363.2
	20140722@364.asc	S8	SS-3 A2 Spot 7	3	−17.0	13.4	0.9	Zone 3	Ank	20.67%	56.66%	19.33%	3.34%	<DL	0.483	0.733	5.0	358.6
	20140722@366.asc	S8	SS-3 A2 Spot 9	3	−15.9	14.5	0.9	Zone 3	Ank	20.67%	56.66%	19.33%	3.34%	<DL	0.484	0.733	8.8	353.5
	20140513@666.asc	S7	SS-3 A2 Spot 1	10	−15.0	15.5	0.4	Zone 3	Ank	22.43%	55.01%	20.03%	2.53%	<DL	0.472	0.710	9.4	352.8
	20140722@358.asc	S8	SS-3 A2 Spot 1	3	−13.8	16.7	0.9	Zone 3	Ank	22.16%	55.69%	18.94%	3.19%	0.03%	0.461	0.715	12.1	349.2
	20130925@336.asc	S1	SS-3 A2 Spot 3	10	−14.5	16.0	0.3	Zone 3	Ank	22.38%	55.54%	19.48%	2.60%	<DL	0.465	0.713	14.9	345.5
	20140722@363.asc	S8	SS-3 A2 Spot 6	3	−15.4	15.1	0.9	Zone 3	Ank	20.50%	55.76%	20.67%	3.07%	<DL	0.502	0.731	17.8	341.6
	20140513@667.asc	S7	SS-3 A2 Spot 2	10	−12.9	17.6	0.4	Zone 3	Ank	23.60%	55.01%	18.85%	2.54%	<DL	0.444	0.700	21.9	336.2
	20140722@362.asc	S8	SS-3 A2 Spot 5	3	−14.2	16.2	0.9	Zone 3	Ank	23.79%	54.70%	18.80%	2.72%	<DL	0.441	0.697	23.5	334.1
	20140722@361.asc	S8	SS-3 A2 Spot 4	3	−13.5	16.9	0.9	Zone 3	Ank	23.79%	54.70%	18.80%	2.72%	<DL	0.441	0.697	27.7	328.5
	20130925@335.asc	S1	SS-3 A2 Spot 2	10	−11.4	19.2	0.3	Zone 3	Ank	26.43%	54.98%	16.87%	1.72%	<DL	0.390	0.675	31.5	323.5
	20140513@668.asc	S7	SS-3 A2 Spot 3	10	−10.2	20.4	0.4	Zone 3	Ank	23.55%	53.35%	19.90%	3.19%	<DL	0.458	0.694	33.0	321.5
	20140722@360.asc	S8	SS-3 A2 Spot 3	3	−10.7	19.9	0.9	Zone 3	Ank	23.79%	54.70%	18.80%	2.72%	<DL	0.441	0.697	33.6	320.7
	20140722@359.asc	S8	SS-3 A2 Spot 2	3	−10.1	20.5	0.9	Zone 3	Ank	23.79%	54.70%	18.80%	2.72%	<DL	0.441	0.697	36.6	316.7
Average					−13.6	16.9	–	–	–	22.73%	55.29%	19.14%	2.84%	0.00%	0.458	0.709	–	–
2SD					4.5	4.5	–	–	–	3.41%	1.88%	1.73%	0.90%	0.02%	0.056	0.036	–	–
Additional areas analyzed†																		
	20140513@669.asc	S7	SS-3 A6 Spot 1	10	−7.1	23.6	0.4	Zone 0	FD	42.30%	50.52%	6.86%	0.31%	0.03%	0.140	0.544	–	–
	20140513@670.asc	S7	SS-3 A6 Spot 2	10	−7.9	22.8	0.4	Zone 0	FD	42.30%	50.52%	6.86%	0.31%	0.03%	0.140	0.544	–	–
	20140513@672.asc	S7	SS-3 A6 Spot 4	10	−5.3	25.4	0.4	Zone 1	Ank	36.60%	51.17%	11.14%	1.09%	<DL	0.233	0.583	–	–
	20130925@333.asc	S1	SS-3 A6 Spot 3	10	−7.4	23.3	0.3	Zone 2	FD	39.35%	51.40%	8.73%	0.53%	<DL	0.182	0.566	–	–
	20130925@332.asc	S1	SS-3 A6 Spot 2	10	−7.3	23.4	0.3	Zone 2	FD	41.05%	51.08%	7.42%	0.45%	<DL	0.153	0.554	–	–
	20140513@673.asc	S7	SS-3 A6 Spot 5	10	−7.0	23.7	0.4	Zone 2	FD	40.58%	51.26%	7.55%	0.61%	<DL	0.157	0.558	–	–
	20130925@331.asc	S1	SS-3 A6 Spot 1	10	−13.5	16.9	0.3	Zone 3	Ank	22.87%	55.03%	19.48%	2.62%	<DL	0.460	0.706	–	–
	20140513@674.asc	S7	SS-3 A6 Spot 6	10	−13.4	17.1	0.4	Zone 3	Ank	22.87%	55.03%	19.48%	2.62%	<DL	0.460	0.706	–	–
	20140513@675.asc	S7	SS-3 A6 Spot 7	10	−13.0	17.5	0.4	Zone 3	Ank	22.67%	53.92%	20.51%	2.90%	<DL	0.475	0.704	–	–
	20140513@676.asc	S7	SS-3 A6 Spot 8	10	−12.6	17.9	0.4	Zone 3	Ank	22.87%	55.03%	19.48%	2.62%	<DL	0.460	0.706	–	–
	20140513@657.asc	S7	SS-3 A9 Spot 16	10	−13.5	16.9	0.4	Zone 3	Ank	23.63%	54.95%	18.68%	2.70%	0.04%	0.442	0.699	–	–
	20130925@348.asc	S1	SS-3 A9 Spot 1	10	−14.1	16.3	0.3	Zone 3	Ank	23.63%	54.95%	18.68%	2.70%	0.04%	0.442	0.699	–	–

Refer to Appendix 3 (supplementary material available as AAPG Datashare 71 at www.aapg.org/datashare). Each SIMS pit has a unique analytical session–specific identification number (e.g., 20130925@289.asc in column 2 followed by S1 in column 3).

Abbreviations: Ank = ankerite; Ca = calcium; Cal = calcite; CL = cathodoluminescence; <DL = below detection limit (Mn: 0.1 wt. %; Sr: 0.1 wt. %); FD = ferroan dolomite; Fe = iron; Mg = magnesium; Mn = manganese; NFD = nonferroan dolomite; SIMS = secondary ion mass spectrometry; Sr = strontium; VPDB = Vienna Peedee belemnite; VSMOW = Vienna standard mean ocean water; 2SD = two standard deviations.

*Distance (μm): this is the transect distance of individual SIMS pits relative to either the detrital quartz grain around which cements progressively developed or the distance relative to the innermost exposed cement zone.

†Composite transect/transect distance (compilation of data from several analyzed regions per sample; see supplementary material available as AAPG Datashare 71 at www.aapg.org/datashare.).

Table 3. Oxygen Isotope-Based Precipitation Temperature Estimates for Early and Late Carbonate Cements in Shaly Sandstone Beds of the Eau Claire Formation Sampled for This Study at Three Cored Localities

Sample Name	Core Identification	Present Depth (ft)	Present Depth (m)	Maximum Burial Depth[§] (ft)	Maximum Burial Depth[§] (km)	Temperature at Maximum Burial[¶]	Early Carbonate Cement $\delta^{18}O$ (‰, VSMOW)	Temperature[††] If $\delta^{18}O$ Pore Fluid = −3‰	Latest Carbonate Cement $\delta^{18}O$ (‰, VSMOW)	Temperature[††] of Precipitation If $\delta^{18}O$ Pore Fluid = −3‰	Temperature[††] of Precipitation If $\delta^{18}O$ Pore Fluid = +2‰	$\Delta^{18}O$ (Early–Late)
Wisconsin arch (shallow burial)												
SS-1	C131467*	277.9	84.7	<1500	<0.5 km	~35°C (95°F)	25‰ (Cal average)	30°C (85°F) (Cal)	–	–	–	–
SS-1	C131467*	277.9	84.7	<1500	<0.5 km	~35°C (95°F)	24‰ (Dol average)	50°C (120°F) (Dol)	–	–	–	–
Basin margin, northern Illinois (intermediate burial)												
SS-2	C12996[†]	1217.3	371.0	~3500	~1 km	~50°C (120°F)	24‰[#] (Dol avg.)	50°C (120°F) (Dol)	18‰ (Ank)	85°C (185°F) (Ank)	130°C (265°F) (Ank)	~6‰
Central Illinois Basin (deep burial)												
SS-3	C4006[‡]	3857	1175.6	~6500	~2 km	~80°C (175°F)	24‰** (Dol avg)	50°C (120°F) (Dol)	14‰ (Ank)	120°C (250°F) (Ank)	180°C (355°F) (Ank)	~10‰

Abbreviations: Ank = ankerite; Cal = calcite; Dol = dolomite; VSMOW = Vienna standard mean ocean water.

*API number (none), Dane County, Wisconsin (Wisconsin Geological and Natural History Survey).

[†]API number 121772131700, Stephenson County, Illinois (Illinois State Geological Survey).

[‡]API number 120190012800, Champaign County, Illinois (Illinois State Geological Survey).

[§]For northern and central Illinois: present-day burial depth + 0.7 km (~2300 ft), after figure 11 in Rowan et al. (2002); for the Wisconsin arch: after Altschaeffl and Harrison (1959).

[¶]Assuming a geothermal gradient of 30°C/km (1.6°F/100 ft) and a surface temperature of 20°C (68°F). Based on Illinois Basin burial and thermal history models of Makowitz (2004), Makowitz et al. (2006), and Rowan et al. (2002) and geotherm constraints from Cluff and Byrnes (1991).

[#]Average of values measured specifically from the dolomite crystal cores of compositional zone 0; see Appendix 3, Plates 1A and 4 (supplementary material available as AAPG Datashare 71 at www.aapg.org/datashare).

**Here we assume that cement zone 0 of sample SS-3 had the same average $\delta^{18}O$ value, prior to recrystallization, as cement zone 0 of sample SS-2. The average value at present is 23‰.

[††]Equilibrium fractionation relationship for dolomite–water of Horita (2014).

A useful constraint in the case of fine-grained, low-permeability and clay mineral–rich sediments is knowledge of the fact that pore fluid $\delta^{18}O$ values tend to progressively increase during burial and heating as a result of water–rock interactions (e.g., as a result of clay mineral diagenesis, specifically the commonplace illitization of detrital smectite; see, e.g., Boles and Franks, 1979; Whitney and Northrop, 1988; Longstaffe, 1989; Foscolos, 1990; Wilkinson et al., 1992; Meunier, 2005). Such sediments tend to rapidly expel pore fluids during the first several kilometers of burial and compaction (e.g., figure 12.4 in Giles, 1997) and remain largely impermeable to the migration of outside fluids that could infiltrate the sediment or sedimentary rock and considerably alter the pore fluid $\delta^{18}O$ value during subsequent stages of burial and/or uplift (e.g., largely impervious to cross-basin migrations of deep basinal fluids or to infiltrations by low-$\delta^{18}O$ meteoric waters).

With the above constraint in mind, we can make certain inferences about the temperature conditions of the Eau Claire Formation during carbonate cementation. We propose the two simple end-member scenarios that follow, and we evaluate the resulting paleotemperature estimates against considerations of maximum burial depths for the Eau Claire Formation in this region (Rowan et al., 2002; Makowitz, 2004; Makowitz et al., 2006). At each sampled locality, the temperatures expected to result from burial (Table 3) were calculated by assuming a surface temperature of 20°C (68°F) (cf., Makowitz, 2004; Makowitz et al., 2006) and a geothermal gradient of 30°C/km (86°F/ft) (in agreement with constraints from biomarker data; see Cluff and Byrnes, 1991). Present-day burial depths of samples from northern and central Illinois (samples SS-2 and SS-3, respectively) were corrected to account for 0.7 km (~2300 ft) of uplift and erosion (after Rowan et al., 2002), and less than 0.5 km (~1500 ft) of additional burial was inferred for the vicinity of the Wisconsin arch (sample SS-1 herein; Altschaeffl and Harrison, 1959; Wilson and Sibley, 1978; Hoholick, 1980).

Scenario 1: The first scenario assumes simply that the O-isotope composition of the pore fluid did not evolve as described above; instead, it remained constant at the approximate average value of early Paleozoic seawater (–3‰; e.g., Veizer et al., 1997; Came et al., 2007; Jaffrés et al., 2007; as assumed in the Illinois Basin quartz cement studies of Pollington et al., 2011 and Hyodo et al., 2014). In this case, the range of carbonate $\delta^{18}O$ values, that is, $\Delta^{18}O$ (early–late) = $\delta^{18}O$ (early) – $\delta^{18}O$ (late), provides a minimum estimate of the relative temperature change during carbonate cementation at each of the sampled localities. On the basin margin in northern Illinois, the measured range of approximately 6‰ amounts to a relative temperature change of approximately 35°C (95°F) (from 50°C to 85°C [120°F to 185°F], sample SS-2; Figure 6; Table 3). Deeper in central Illinois, the observed difference of approximately 10‰ in carbonate $\Delta^{18}O$ (early–late) amounts to a change in temperature of approximately 70°C (160°F) (from 50°C to 120°C [120°F to 250°F], sample SS-3; Figure 6; Table 3).

In this scenario, the NFD cement observed on the Wisconsin arch (sample SS-1) began precipitating at a burial temperature of approximately 50°C (120°F) (Figure 6; Table 3). Calcite cement is also present at this locality but may not be primary. Its coarse, sparry texture is suggestive of recrystallization, which in this scenario would have occurred at temperatures of approximately 30°C (85°F). Based on the occurrence of what appear to be dolomitization fronts infringing upon calcite crystal boundaries (Appendix 3, Plate 2A–D [supplementary material available as AAPG Datashare 71 at www.aapg.org/datashare]), it is possible that a precursory calcite cement existed before the precipitation of the earliest dolomite cement. In the shaly sandstone beds of the basin margin in northern Illinois (sample SS-2), the average $\delta^{18}O$ value of the earliest identified dolomite crystal cores (zone 0) yields a temperature estimate of 50°C (120°F) (Figure 6; Table 3). Because of apparent recrystallization, these same dolomite crystal cores are no longer discernable at depth in central Illinois (sample SS-3). The lowest $\delta^{18}O$ values measured near the rims of the final generation of carbonate cement (ankerite zone 3) correspond to a temperature of approximately 85°C (185°F) (SS-2, paleodepth ~1 km [3500 ft]) on the basin margin and to a temperature of approximately 120°C (250°F) deeper in central Illinois (sample SS-3, paleodepth ~2 km [6500 ft]; Table 3).

Scenario 2: The second scenario assumes that the O-isotope composition of the pore fluid had progressively evolved away from the starting value of –3‰ (scenario 1) as a result of clay mineral

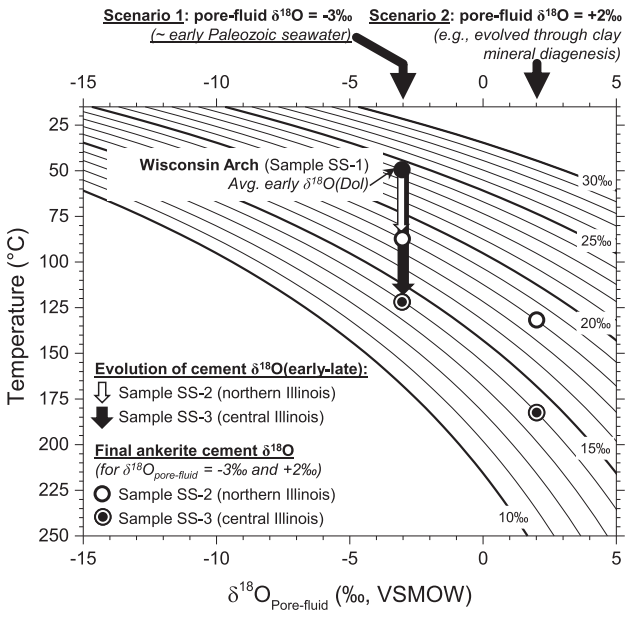

Figure 6. Plot relating measured $\delta^{18}O$ values of dolomite–ankerite cements to temperature of formation (°C) as a function of different pore fluid $\delta^{18}O$ values (equilibrium fractionation relationship of Horita, 2014). The subparallel lines stretching across the plot are isopleths, or lines of constant cement $\delta^{18}O$ values (e.g., a cement $\delta^{18}O$ value of 14‰ may result from different temperature and pore fluid $\delta^{18}O$ conditions). To a first order, the $\delta^{18}O$ values of chemo-isotopically zoned dolomite–ankerite cements within the shaly sandstone beds of the predominantly silty–shaly Eau Claire Formation progressively evolve from approximately 24‰ to approximately 18‰ on the basin margin in northern Illinois (sample SS-2) and from approximately 24‰ to approximately 14‰ in the central Illinois Basin (sample SS-3). The range of cement precipitation temperatures is discussed in terms of two end-member scenarios (see text). Avg. = average; Dol = dolomite; VSMOW = Vienna standard mean ocean water.

diagenesis by the time interval during which the latest generation of carbonate cement precipitated (ankerite zone 3). The illitization of smectite clays in Eau Claire shale beds, adjacent to the shaly sandstone intervals of interest, has progressed to an advanced stage in samples from shallow and deep burial alike (<15% smectite remains, Table 1). The progression of this reaction would have imparted a positive shift in the pore fluid $\delta^{18}O$ value, although we cannot in the present case quantify the magnitude of this change. However, a change of up to +5‰–10‰ could be reasonably expected based on studies concerning the evolution of oxygen isotope ratios in the pore fluids of other mudrocks (e.g., Wilkinson et al., 1992; see also Whitney and Northrop, 1988). If we assume a change on the lower end of this range (+5‰, because the Eau Claire is not as clay rich as the above cited examples), then the lowest $\delta^{18}O$ values measured near the crystal rims of the final ankerite cement correspond to a temperature of approximately 130°C (265°F) on the basin margin in northern Illinois and to a temperature of approximately 180°C (355°F) at depth in central Illinois (Figure 6; Table 3). In this second scenario, the temperature estimates fall near the high end of paleotemperature measurements from fluid inclusions that represent the warmest stages of mineralization in both the Upper Mississippi Valley district in northern Illinois (~100°C–150°C [210°F–300°F]) and the Fluorspar district in southern Illinois (~135°C–175°C [275°F–350°F]; see figures 11, 12 in Rowan et al., 2002).

Late-Stage Ankerite Cementation at Circa 270 Ma (Mississippi Valley–Type Event)?

In both of the above proposed end-member scenarios, the $\delta^{18}O$-based precipitation temperature estimates for the final ankerite cement (zone 3) are anomalously high relative to burial model predictions for the basin margin in northern Illinois and for the burial depths of the Eau Claire Formation in central Illinois (burial temperatures exceeded by approximately 35°C–40°C [95°F–105°F] in scenario 1 and by approximately 80°C–100°C [175°F–210°F] in scenario 2; Table 3). This can be plausibly explained within the context of the model proposed by Rowan et al. (2002), where hydrothermal heating associated with the early to mid-Permian MVT event is identified as an important component in understanding the thermal evolution of the Illinois Basin, especially the anomalously advanced diagenetic maturity of its strata in relation to maximum estimated burial depths and associated temperatures (see the Burial and Thermal History of the Illinois Basin section). The final stage of carbonate cementation, mainly the precipitation of the distinctly Fe-rich ankerite (cement zone 3), may well have overlapped in time with conductive heating (cf., Rowan et al., 2002) of the Eau Claire Formation from under- and overlying sandstone aquifers that channeled the flow of hot mineralizing brines

(~100°C–175°C [210°F–350°F]) at circa 270 Ma, that is, the approximate age of formation of regional MVT lead and zinc ore districts. Because of its largely aquitard-like character (e.g., Lahann et al., 2014), the pore fluids of the Eau Claire Formation likely remained isolated from direct contact with these brines (i.e., the pore fluid $\delta^{18}O$ value is unlikely to have been considerably altered by mixing with hydrothermal brines, the composition of which remains poorly constrained).

The basin-wide precipitation of the distinctly Fe-rich, late-stage ankerite cement would have required a considerable abundance of dissolved Fe^{2+} and Mg^{2+} in the pore fluid at the time of precipitation. The anomalously advanced diagenetic maturity of clay minerals within Eau Claire Formation shale beds offers a tenable explanation. Specifically, illite in lower Paleozoic strata of the Illinois Basin, below the Ordovician Maquoketa Shale, is comprised predominantly of diagenetic (the polytypes $1M_d$ and 1M) rather than detrital ($2M_1$) varieties (Grathoff et al., 2001; Kunle Dare, 2004). A major episode of illite formation was previously dated via the K–Ar method to circa 300–250 Ma, whereas kinetic models of smectite illitization indicate that the highly illitic nature of clays throughout the basin is unlikely to be the sole result of progressive sediment burial and heating (Elliott and Aronson, 1993; Grathoff et al., 2001). Grathoff et al. (2001) proposed that hydrothermal activity drove the reaction of smectite to illite to a stage more advanced than can be accounted for by "normal" burial diagenesis, and topographically driven fluid flow was implicated in having flushed hot brines (<140°C [285°F]) across the Illinois Basin during uplift of the Ouachita orogenic belt; this is conceptually analogous to the model of Rowan et al. (2002) and the earlier studies upon which it was developed. Among the common diagenetic reactions of volumetric significance in mixed sandstone–shale systems, the progressive illitization of detrital smectites (S → I) is of particular importance as a source of dissolved Fe^{2+} and Mg^{2+} for the formation of increasingly Fe-rich dolomite–ankerite cements during progressive sediment burial and heating (e.g., Boles and Franks, 1979; Foscolos, 1990; Nesse, 2000; Meunier, 2005; Milliken, 2003; Morad et al., 2003). The S → I reaction can be qualitatively expressed as

$$K^+ + \text{smectite layers in mixed illite–smectite} \rightarrow \text{illite layers in mixed illite–smectite} + \text{silica} + \text{other products (including } Ca^{2+},\ Mg^{2+},\ Fe^{2+},\ H_2O)$$

(after Boles and Franks, 1979; Foscolos, 1990). It is thought that Fe- and/or Mg-rich smectite layers do not react as readily to form illite as do the more aluminous and Ca-rich smectite compositions; the large-scale illitization of the former is thought to occur near the upper end (~125°C [260°F]; e.g., Boles and Franks, 1979) of the temperature range proposed for this reaction (60°C–140°C [140°F–285°F]; e.g., Milliken, 2003) and to be accompanied by the release of volumetrically significant quantities of aqueous Fe^{2+} and Mg^{2+} into pore fluids (Boles and Franks, 1979). Given sufficient pore fluid alkalinity, the aqueous by-products of the S → I reaction facilitate dolomite–ankerite cementation not only in host shale beds but also in adjacent or interbedded sandstones through the mass transfer that accompanies the dewatering of shales via compaction and dehydration of clay minerals (e.g., Boles and Franks, 1979; Pollastro, 1985; Foscolos, 1990; Macaulay et al., 1992; Surdam and Yin, 1994; Hendry, 2002; Schmid et al., 2004; Machent et al., 2007; Krajewski and Woźny, 2009). This reaction also constitutes a significant source of dissolved silica for the formation of quartz overgrowths, in addition to the supply from pressure solution in adjacent sandstone beds (Boles and Franks, 1979). Thus, in response to conductive heating of the Eau Claire Formation during the early to mid-Permian MVT event, the breakdown of Fe- and Mg-rich smectite clays within the shale beds of this lithologically heterogeneous unit could have potentially comprised an internal source of ions for carbonate cementation.

Timing of Carbonate Cementation

When integrated with existing burial and thermal history models for the Illinois Basin (those independently constrained by Rowan et al., 2002; Makowitz et al., 2006), the range of $\delta^{18}O$-based temperature estimates (calculated via either scenario 1 or 2) suggests that carbonate cements began precipitating soon after deposition of the Upper Cambrian Eau Claire Formation. Cementation

continued, perhaps only intermittently, into the early to mid-Permian (Table 3), with the final stage of carbonate precipitation in this closed system overlapping in time with conductive heating of the unit from under- and overlying sandstone aquifers that channeled hydrothermal fluids responsible for regional MVT mineralization (ca. 270 Ma). In an overarching sense, this time interval (Upper Cambrian–early to mid-Permian) in the tectonic history of the basin is characterized by a prolonged episode of subsidence and marine sedimentation (e.g., Kolata and Nelson, 2010). The first-order decrease in cement $\delta^{18}O$ values observed in core-to-rim transects across patches of zoned dolomite–ankerite (Figure 4) is consistent with cement growth at progressively higher temperatures (Figure 6). The $\delta^{18}O$ trends do not, however, rebound back toward higher values near the crystal rims (i.e., toward lower precipitation temperatures). Therefore, it seems reasonable to suspect that carbonate cementation ended before the onset of uplift-related cooling that began in the late Permian (Makowitz et al., 2006).

A final note concerns the very earliest dolomite cement examined in this study. Mainly, the observed first-order decrease of carbonate $\delta^{18}O$ values over the course of the carbonate cementation history (zone $0 \rightarrow 1 \rightarrow 2 \rightarrow 3$) has superimposed on it higher order variations during the early stages of dolomite precipitation (zone 0), where values range between 19.5‰ and 28‰ in the shaly sandstone beds of the basin margin in northern Illinois and between 21‰ and 25‰ in central Illinois (Figure 4). Further, the dispersed dolomite cement crystals in the shaly sandstone beds of the shallowly buried Wisconsin arch (<0.5 km [1500 ft]) record a conspicuous shift in $\delta^{18}O$ values, where crystallite rims are more positive by 5‰ compared with the earlier-formed cores (the CL-light versus CL-dim domains, respectively; Figure 5B, E, F). This shift is opposite in direction to $\delta^{18}O$ trends that arise because of temperature increases during progressive sediment burial. Changes in pore fluid $\delta^{18}O$ values are a more plausible means of producing such shifts in carbonate $\delta^{18}O$ and are characteristic of coastal, shallow-burial environments where marine and isotopically light meteoric waters mix to a varying extent (e.g., see Craig, 1961; Badiozamani, 1973; Folk and Land, 1975; Magaritz et al., 1980; Barlow, 2003). For dolomite precipitation temperature estimates to be consistent with burial model predictions for the vicinity of the Wisconsin arch (Table 3), pore fluid $\delta^{18}O$ values in the range of –5‰ to –10‰ would have been required in the mixing zone (Figure 6). This is plausible, given that we could reasonably expect that the $\delta^{18}O$ value of meteoric waters entering the mixing zone would have fallen in the range of –5‰ and –10‰ (based on trends in the O-isotope composition of oil-field waters from various North American basins and the intersection of these trends with the global meteoric water line; e.g., Kharaka and Hanor, 2003; Labotka et al., 2015).

THE APPLICABILITY OF SECONDARY ION MASS SPECTROMETRY IN CARBON SEQUESTRATION RESEARCH

A Method for Identifying Carbonate Cements That Form in Response to Carbon Dioxide Injection at Carbon Sequestration Sites

A desirable consequence of supercritical CO_2 injection into saline sandstone reservoirs at prospective sites for geologic carbon capture and storage (CCS) is the eventual precipitation of carbonate mineral cements and hence permanent storage of some part of the injected CO_2. At the IBDP, a demonstration site for the feasibility of long-term carbon sequestration (Leetaru et al., 2009; US Department of Energy, 2010; Leetaru and Freiburg, 2014), it has been estimated that at least 10%–20% of the introduced CO_2 may be consumed in the precipitation of Fe carbonates (Finley, 2005; Liu et al., 2011; Carroll et al., 2013). Distinguishing the carbonate cements that form in response to CO_2 injection from those that already locally occupy the pore space will require establishing a preinjection point of reference. A necessary component of such a preinjection baseline would be a comprehensive petrographic characterization of the carbonate cements that formed in both the reservoir unit (Mt. Simon) and in the reservoir seal rock (Eau Claire Formation) during sediment diagenesis. Such a characterization by petrographic means could be buttressed by fingerprinting the chemical and isotopic ($\delta^{13}C$ and $\delta^{18}O$) compositions of existing cement generations.

The reconnaissance study of Neufelder et al. (2012) indicates that carbonate cements are abundant

in the Eau Claire Formation, although the diversity of lithofacies that comprise this unit, together with their heterogeneous spatial distribution (Lahann et al., 2014), necessitates further petrographic study, ideally employing a combination of complementary imaging techniques (e.g., optical microscopy complemented by CL and BSE imaging by means of SEM). Volumetrically significant abundances of carbonate cement also occur locally throughout the Mt. Simon Sandstone, although such cements are predominantly concentrated near the boundary with the overlying Eau Claire Formation. Mineralogically, these cements belong to the dolomite–ankerite and the siderite to Mg–siderite solid solution series. Following injection, it is anticipated that the emplaced CO_2 plume will expand and rise upward until it encounters the impermeable Eau Claire Formation, and will subsequently spread out along this interface between and the reservoir and the seal rock. Permanent storage of a part of the injected CO_2 via carbonate mineral precipitation is expected especially in this particular zone of the reservoir as the CO_2 plume reacts chemically with the base of the Eau Claire Formation (Finley, 2005).

Recent advances in carbonate mineral analysis by SIMS are a potentially pertinent development for future monitoring studies at CCS sites, which may seek to (1) verify whether carbonate cements are indeed forming in response to CO_2 injection, (2) quantify their abundance and delimit their spatial distribution, and/or (3) determine, by isotopic fingerprinting, if fracture filling cements in either the reservoir or seal rock are related to CO_2 plume migration. Here, the SIMS technique can contribute uniquely, because it allows for micrometer-scale measurements of $\delta^{18}O$ and $\delta^{13}C$ to be made in situ from thin sections, 1-in.-diameter core plugs, or cuttings (Valley and Kita, 2009). This technique would be particularly applicable in a case where sequestration-induced carbonate cements form in pore space already partially occupied by carbonate cements of diagenetic origin and where mechanical separation of the two is not possible in the preparation of samples for isotopic analysis by conventional drilling techniques.

If any particular type of carbonate cement encountered in the course of future monitoring studies is suspected on a petrographic basis of having formed in response to CO_2 injection at sequestration sites, it may well exhibit an isotopic signature that uniquely distinguishes it from preexisting carbonate cements of diagenetic origin. In the presence of certain pieces of supporting data, it is possible to foretell the probable $\delta^{13}C$ and $\delta^{18}O$ values of the different carbonate minerals that may precipitate within the reservoir or seal rock by employing mineral–water and mineral–CO_2 equilibrium fractionation relationships. This includes (1) knowledge concerning ambient reservoir conditions (e.g., temperature and brine composition to correct for any known isotope salt effects, cf., Horita et al., 1993a, b) and (2) a characterization of isotopic composition ($\delta^{13}C$ and $\delta^{18}O$) of both the formation water and the injected CO_2. Such modeling, however, is beyond the scope of the present study.

As a first step toward enabling the above-mentioned monitoring studies and toward establishing a preinjection cementation baseline, we have developed procedures for carbonate microanalysis by SIMS and a suite of reference materials to analyze carbonate compositions that fall along the dolomite–ankerite solid solution series (Śliwiński et al., 2015a, b). An important aspect of further advancing analytical methods is the continued development of reference materials to correct for SIMS-specific sample matrix effects in the analysis of Ca–Mg–Fe carbonates; efforts at present are focused on the magnesite–siderite solid solution series.

CONCLUSIONS

1. Recent advances in SIMS analytical methods allow for in situ measurements of carbonate mineral $\delta^{18}O$ values from sample domains that are 3–10 μm in diameter (by ~1–2 μm deep) with a high degree of accuracy and precision. Progress on this front significantly increases the spatial resolution available to studies of diagenesis in sandstone–shale and carbonate systems. These technical advances also have applicability in future monitoring studies at carbon capture and storage (sequestration) sites. For example, isotopic fingerprint via coupled $\delta^{18}O$ and $\delta^{13}C$ analyses (e.g., Śliwiński et al., 2015c), could be performed to (1) verify whether carbonate cements are indeed forming in response to CO_2 injection, (2) delimit their spatial distribution and aid in abundance quantification, and/or (3) determine if

fracture filling cements in either the reservoir or seal rock are related to CO_2 plume migration.

2. The history of carbonate cementation in the Upper Cambrian Eau Claire Formation of the Illinois Basin was investigated as a case study, employing $\delta^{18}O$ values measured from chemo-isotopically zoned dolomite–ankerite cements as a proxy record of sediment burial temperatures. Shaly sandstone beds within this predominantly silty-shaly lithofacies package were sampled at three cored localities that represent different paleodepths: (1) the Wisconsin arch (<0.5 km [~1500 ft]), (2) the basin margin in northern Illinois (~1 km [3500 ft]), and (3) at depth in central Illinois (~2 km [6500 ft]). Four major stages of progressive cement development were identified on the basis of discrete changes in cation chemistry: zone 0 (NFD), zone 1 (ankerite), zone 2 (FD → ankerite), and zone 3 (latest, most Fe-rich ankerite). Measurements along transects (100–375 μm long) extending from early to late generations of cement reveal that, to a first order, cement $\delta^{18}O$ values systematically decrease. We observed a difference of approximately 6‰ between early dolomite and late ankerite (i.e., $\Delta^{18}O$ [Early–Late]) on the basin margin (values grade from 24‰ to 18‰, VSMOW/–6.5‰ to –12.5‰ VPDB) and a difference of approximately 10‰ at depth in central Illinois (value grade from 24‰ to 14‰/–6.5‰ to –16.5‰ VPDB). The simplest explanation that can be offered for this trend is that it primarily reflects temperature increases during diagenesis.
3. We considered two end-member scenarios to estimate the range of temperatures over which carbonate cementation occurred. In scenario 1 (constant pore fluid $\delta^{18}O$ value of –3‰, i.e., approximately that of early Paleozoic seawater), cement precipitation temperatures extend from approximately 50°C (120°F) (earliest dolomite) to 85°C (185°F) (latest ankerite) on the basin margin in northern Illinois and to 120°C (250°F) in central Illinois. In scenario 2 (pore fluid $\delta^{18}O$ value evolves by +5‰ as a result of clay mineral diagenesis), cement precipitation temperatures extend from approximately 50°C (120°F) (earliest dolomite) to 130°C (265°F) (latest ankerite) on the basin margin in northern Illinois and to 180°C (355°F) in central Illinois. In both scenarios, the $\delta^{18}O$-based precipitation temperature estimates for the final ankerite cement (zone 3) exceed burial model predictions by a minimum of 35°C–40°C (95°F–105°F) and a maximum of 80°C–100°C (175°F–210°F).
4. The final stage of carbonate cementation—the precipitation of a distinctly Fe-rich ankerite cement zone (3)—is inferred to have overlapped in time with conductive heating of the Eau Claire Formation from under- and overlying sandstone aquifers that channeled the flow of hot brines at circa 270 Ma, during regional MVT lead and zinc ore mineralization.
5. When integrated with the independently constrained burial and thermal history model for the Illinois Basin proposed by Rowan et al. (2002), the range of estimated temperatures indicates that carbonate cements began precipitating soon after deposition during the Late Cambrian and continued developing intermittently into the mid-Permian (until ca. 270 Ma); cementation ended before the onset of uplift-related cooling beginning in the late Permian (cf., Makowitz, 2004; Makowitz et al., 2006).

REFERENCES CITED

Altschaeffl, A. G., and W. Harrison, 1959, Estimation of a minimum depth of burial for a Pennsylvanian underclay: Journal of Sedimentary Petrology, v. 29, p. 178–185, doi: 10.1306/74D708C6-2B21-11D7-8648000102C1865D.

Arthur, M. A., T. F. Anderson, I. R. Kaplan, J. Veizer, and L. S. Land, 1983, Stable isotopes in sedimentary geology: Tulsa, Oklahoma, SEPM Short Course Notes 10, doi:10.2110/scn.83.10.

Aswasereelert, W., 2005, Facies distribution and stacking of the Eau Claire Formation, Wisconsin: Implications of thin shale-rich strata in fluid flow, Master's thesis, University of Wisconsin–Madison, Madison, Wisconsin, 200 p.

Aswasereelert, W., J. A. Simo, and D. L. LePain, 2008, Deposition of the Cambrian Eau Claire Formation, Wisconsin: Hydrostratigraphic implications of fine-grained cratonic sandstones: Geoscience Wisconsin, v. 19, no. 1, p. 1–21.

Badiozamani, K., 1973, The Dorag dolomitization model—Application to the Middle Ordovician of Wisconsin: Journal of Sedimentary Petrology, v. 43, no. 4, p. 965–984.

Barlow, P. M., 2003, Ground water in freshwater-saltwater environments of the Atlantic Coast: US Geological Survey Circular, v. 1262, p. 1–21.

Bethke, C. M., 1985, A numerical model of compaction-driven groundwater flow and heat transfer and its application to the paleohydrology of intracratonic sedimentary basins: Journal of Geophysical Research, v. 90, p. 6817–6828, doi:10.1029/JB090iB08p06817.

Bethke, C. M., 1986, Hydrologic constraints on the genesis of the Upper Mississippi Valley mineral district from Illinois basin brines: Economic Geology and the Bulletin of the Society of Economic Geologists, v. 81, p. 233–249, doi:10.2113/gsecongeo.81.2.233.

Bethke, C. M., 1989, Modeling subsurface flow in sedimentary basins: Geologische Rundschau, v. 78, p. 129–154, doi:10.1007/BF01988357.

Bethke, C. M., and S. Marshak, 1990, Brine migrations across North America—The plate tectonics of groundwater: Annual Review of Earth and Planetary Sciences, v. 18, p. 287–315, doi:10.1146/annurev.ea.18.050190.001443.

Bickle, M., N. Kampman, and M. Wigley, 2013, Natural analogues, *in* D. J. DePaolo, D. R. Cole, A. Navrotsky, and I. C. Bourg, eds., Geochemistry of geologic CO_2 sequestration: Reviews in Mineralogy and Geochemistry 77, p. 15–71.

Boles, J. R., and S. G. Franks, 1979, Clay diagenesis in Wilcox Sandstones of Southwest Texas: Implications of smectite diagenesis on sandstone cementation: Journal of Sedimentary Petrology, v. 49, no. 1, p. 55–70.

Came, R. E., J. M. Eiler, J. Veizer, K. Azmy, U. Brand, and C. R. Weidman, 2007, Coupling of surface temperatures and atmospheric CO_2 concentrations during the Palaeozoic era: Nature, v. 449, no. 7159, p. 198–201, doi:10.1038/nature06085.

Carroll, S. A., W. W. McNab, Z. Dai, and S. C. Torres, 2013, Reactivity of Mount Simon Sandstone and the Eau Claire Shale under CO_2 storage conditions: Environmental Science and Technology, v. 47, p. 252–261, doi:10.1021/es301269k.

Chang, L. L. Y., R. A. Howie, and J. Zussman, 1996, Rock forming minerals, v. 5B: Non-silicates: Sulphates, carbonates, phosphates and halides, 2nd ed.: London, Longman Group, 383 p.

Chen, Z., 2001, Diagenesis of Upper Cambrian Mount Simon Sandstone in the Illinois Basin—Microscale investigation of basinal fluid migration and mass transfer, Ph.D. dissertation, University of Tennessee–Knoxville, Knoxville, Tennessee, 170 p.

Cluff, R. M., and A. P. Byrnes, 1991, Lopatin analysis of maturation and petroleum generation in the Illinois Basin, *in* M. W. Leighton, D. R. Kolata, D. F. Oltz, and J. J. Eidel, eds., Interior cratonic basins: AAPG Memoir 51, p. 425–454.

Craig, H., 1961, Isotopic variations in meteoric waters: Science, v. 133, no. 3465, p. 1702–1703, doi:10.1126/science.133.3465.1702.

Dutton, S. P., and L. S. Land, 1985, Meteoric burial diagenesis of Pennsylvanian arkosic sandstones, Southwestern Anadarko Basin, Texas: AAPG Bulletin, v. 69, no. 1, p. 22–38.

Elliott, W. C., and J. L. Aronson, 1993, The timing and extent of illite formation in Ordovician K-bentonites at the Cincinnati arch, the Nashville dome and north-eastern Illinois basin: Basin Research, v. 5, p. 125–135, doi:10.1111/j.1365-2117.1993.tb00061.x.

Fayek, M., M. Harrison, M. Grove, K. D. McKeegan, C. D. Coath, and J. R. Boles, 2001, In situ stable isotopic evidence for protracted and complex carbonate cementation in a petroleum reservoir, North Coles Levee, San Joaquin Basin, California, U.S.A.: Journal of Sedimentary Research, v. 71, no. 3, p. 444–458, doi:10.1306/2DC40954-0E47-11D7-8643000102C1865D.

Finley, R., 2005, An assessment of geological carbon sequestration options in the Illinois Basin: Phase I final report: Midwest Geological Sequestration Consortium, accessed October 5, 2015, http://www.sequestration.org/resources/reports.html.

Fishman, N. S., 1997, Basin-wide fluid movement in a Cambrian paleoaquifer—Evidence from the Mt. Simon Sandstone, Illinois and Indiana, *in* I. P. Montañez, J. M. Gregg, and K. L. Shelton, eds., Basin-wide diagenetic patterns: Integrated petrologic, geochemical, and hydrologic consideration: Tulsa, Oklahoma, SEPM Special Publication 57, p. 221–234, doi:10.2110/pec.97.57.0221.

Folk, R. L., and L. S. Land, 1975, Mg/Ca ratio and salinity: Two controls over crystallization of dolomite: AAPG Bulletin, v. 59, no. 1, p. 60–68.

Foscolos, A. E., 1990, Catagenesis of argillaceous sedimentary rocks, *in* I. A. McIlreath and D. W. Morrow, eds., Diagenesis: St. John's, Newfoundland, Canada, Geological Association of Canada, p. 177–189.

Giles, M. R., 1997, Diagenesis: A quantitative perspective—Implications for basin modelling and rock property prediction: Dordrecht, The Netherlands, Kluwer Academic Publishers, 526 p.

Grathoff, G. H., D. M. Moore, R. L. Hay, and K. Wemmer, 2001, Origin of illite in the lower Paleozoic of the Illinois Basin: Evidence for brine migrations: Geological Society of America Bulletin, v. 113, no. 8, p. 1092–1104, doi:10.1130/0016-7606(2001)113<1092:OOIITL>2.0.CO;2.

Hendry, J. P., 2002, Geochemical trends and palaeohydrological significance of shallow burial calcite and ankerite cements in Middle Jurassic strata on the East Midlands Shelf (onshore UK): Sedimentary Geology, v. 151, p. 149–176, doi:10.1016/S0037-0738(01)00236-6.

Hervig, R. L., P. Williams, R. M. Thomas, S. N. Schauer, and I. M. Steele, 1992, Microanalysis of oxygen isotopes in insulators by secondary ion mass spectrometry: International Journal of Mass Spectrometry and Ion Processes, v. 120, p. 45–63, doi:10.1016/0168-1176(92)80051-2.

Hoholick, J. D., 1980, Porosity, grain fabric, water chemistry, cement, and depth of the St. Peter Sandstone in the Illinois Basin, Master's thesis, University of Cincinnati, Cincinnati, Ohio, 72 p.

Horita, J., 2014, Oxygen and carbon isotope fractionation in the system dolomite–water–CO_2 to elevated temperatures: Geochimica et Cosmochimica Acta, v. 129, p. 111–124, doi:10.1016/j.gca.2013.12.027.

Horita, J., D. R. Cole, and D. J. Wesolowski, 1993a, The activity-composition relationship of oxygen and hydrogen isotope in aqueous salt solutions: II. Vapor-liquid water equilibration of mixed salt solutions from 50 to 100°C and geochemical implications: Geochimica et Cosmochimica Acta, v. 57, p. 4703–4711, doi:10.1016/0016-7037(93)90194-2.

Horita, J., D. J. Wesolowski, and D. R. Cole, 1993b, The activity-composition relationship of oxygen and hydrogen isotope in aqueous salt solutions: I. Vapor-liquid water equilibration of single salt solutions from 50 to 100°C: Geochimica et Cosmochimica Acta, v. 57, p. 2797–2817, doi:10.1016/0016-7037(93)90391-9.

Hyodo, A., R. Kozdon, A. D. Pollington, and J. W. Valley, 2014, Evolution of quartz cementation and burial history of the Eau Claire Formation based on in situ oxygen isotope analysis of quartz overgrowth: Chemical Geology, v. 384, p. 168–180, doi:10.1016/j.chemgeo.2014.06.021.

Jaffrés, J. B. D., G. A. Shields, and K. Wallmann, 2007, The oxygen isotope evolution of seawater: A critical review of a long-standing controversy and an improved geological water cycle model for the past 3.4 billion years: Earth-Science Reviews, v. 83, p. 83–122, doi:10.1016/j.earscirev.2007.04.002.

Kharaka, Y. K., and J. S. Hanor, 2003, Deep fluid in the continents: 1. Sedimentary basins, *in* J. I. Drever, ed., Treatise on geochemistry, v. 5: Surface and groundwater, weathering and soils: Oxford, United Kingdom, Elsevier, p. 499–540.

Kita, N. T., T. Ushikubo, B. Fu, and J. W. Valley, 2009, High precision SIMS oxygen isotope analysis and the effect of sample topography: Chemical Geology, v. 264, p. 43–57, doi:10.1016/j.chemgeo.2009.02.012.

Kolata, D. R., 2005, Bedrock geology of Illinois: Illinois State Geological Survey Illinois Map 14, scale 1:500,000, 2 sheets.

Kolata, D. R., and W. J. Nelson, 2010, Tectonic history, *in* D. R. Kolata and C. K. Nimz, eds., Geology of Illinois: Champaign, Illinois, University of Illinois at Urbana-Champaign, Institute of Natural Resource Sustainability, Illinois State Geological Survey, p. 77–89.

Krajewski, K. P., and E. Woźny, 2009, Origin of dolomite-ankerite cement in the Bravaisberget Formation (Middle Triassic) in Spitzbergen, Svalbard: Polish Polar Research, v. 30, no. 3, p. 231–248, doi:10.4202/ppres.2009.11.

Kunle Dare, M. A., 2004, Relationship between reservoir properties of the Galesville Sandstone and diagenesis of Eau Claire Shale, Cambrian of Illinois Basin (abs.): AAPG Annual Meeting, Dallas, Texas, April 18–21, 2004, accessed November 19, 2014, http://www.searchanddiscovery.com/abstracts/html/2004/annual/abstracts/Kunle.htm.

Labotka, D. M., S. V. Panno, R. A. Locke, and J. T. Freiburg, 2015, Isotopic and geochemical characterization of fossil brines of the Cambrian Mt. Simon Sandstone and Ironton–Galesville Formation from the Illinois Basin, USA: Geochimica et Cosmochimica Acta, v. 165, p. 342–360, doi:10.1016/j.gca.2015.06.013.

Lahann, R., J. Rupp, and C. Medina, 2014, An evaluation of the seal capacity and CO_2 retention properties of the Eau Claire Formation (Cambrian): Environmental Geoscience, v. 21, no. 3, p. 83–106, doi:10.1306/eg.05011414003.

Leetaru, H. E., S. Frailey, D. Morse, and R. J. Finley, 2009, Carbon sequestration in the Mt. Simon sandstone saline reservoir, *in* M. Grobe, J. C. Pashin, and R. L. Doge, eds., Carbon dioxide sequestration in geological media—State of the science: AAPG Studies in Geology 59, p. 261–277.

Leetaru, H. E., and J. T. Freiburg, 2014, Litho-facies and reservoir characterization of the Mt Simon Sandstone at the Illinois Basin–Decatur Project: Greenhouse Gases: Science and Technology, v. 4, p. 580–595, doi:10.1002/ghg.1453.

Liu, F., P. Lu, C. Zhu, and Y. Xiao, 2011, Coupled reactive flow and transport modeling of CO_2 sequestration in the Mount Simon sandstone formation, Midwest U.S.A.: International Journal of Greenhouse Gas Control, v. 5, p. 294–307, doi:10.1016/j.ijggc.2010.08.008.

Longstaffe, F. J., 1989, Stable isotopes as traces in clastic diagenesis, *in* I. E. Hutcheon, ed., Burial diagenesis: Mineralogical Association of Canada Short Course Handbook 15, p. 201–277.

Macaulay, C. I., R. S. Haszeldine, and A. E. Fallick, 1992, Distribution, chemistry, isotopic composition and origin of diagenetic carbonates: Magnus Sandstone, North Sea: Journal of Sedimentary Petrology, v. 63, no. 1, p. 33–43.

Machel, H. G., 1997, Recrystallization versus neomorphism, and the concept of 'significant recrystallization' in dolomite research: Sedimentary Geology, v. 113, p. 161–168, doi:10.1016/S0037-0738(97)00078-X.

Machent, P. G., K. G. Taylor, J. H. S. Macquaker, and J. D. Marshall, 2007, Patterns of early post-depositional and burial cementation in distal shallow-marine sandstones: Upper Cretaceous Kenilworth Member, Book Cliffs, Utah, USA: Sedimentary Geology, v. 198, p. 125–145, doi:10.1016/j.sedgeo.2006.12.002.

Magaritz, M., L. Goldenberg, U. Kafri, and A. Arad, 1980, Dolomite formation in the seawater-freshwater interface: Nature, v. 287, p. 622–624, doi:10.1038/287622a0.

Makowitz, A., 2004, The genetic association between brittle deformation and quartz cementation: Examples from burial compaction and cataclasis, Ph.D. dissertation, The University of Texas at Austin, Austin, Texas, 298 p.

Makowitz, A., R. H. Lander, and K. L. Milliken, 2006, Diagenetic modeling to assess the relative timing of quartz cementation and brittle grain processes during compaction: AAPG Bulletin, v. 90, no. 6, p. 873–885, doi:10.1306/12190505044.

Meunier, A., 2005, Clays: Berlin, Germany, Springer-Verlag, 472 p.

Milliken, K. L., 2003, Late diagenesis and mass transfer in sandstone–shale sequences, *in* F. Mackenzie, ed., Treatise on geochemistry, v. 7: Sediments, diagenesis, and sedimentary rocks: Amsterdam, The Netherlands, Elsevier, p. 159–190, doi:10.1016/B0-08-043751-6/07091-2.

Moorehead, A. J., 2013, Igneous intrusions at the Hicks Dome, southern Illinois, and their relationship to fluorine-base metal-rare earth element mineralization, Master's thesis, Southern Illinois University Carbondale, Carbondale, Illinois, 226 p.

Morad, S., R. H. Worden, and J. M. Ketzer, 2003, Oxygen and hydrogen isotopic composition of diagenetic clay minerals in sandstones: A review of the data and controls, *in* R. H. Worden and S. Morad, eds., Clay mineral cements in sandstones: International Association of Sedimentologists Special Publication 34, p. 63–91.

Nelson, W. J., 1991, Structural styles of the Illinois Basin, *in* M. W. Leighton, D. R. Kolata, D. F. Oltz, and J. J. Eidel, eds., Interior cratonic basins: AAPG Memoir 51, p. 209–243.

Nesse, W. D., 2000, Introduction to mineralogy: New York, Oxford University Press, 442 p.

Neufelder, R. J., B. B. Bowen, R. W. Lahann, and J. A. Rupp, 2012, Lithologic, mineralogical and petrophysical characteristics of the Eau Claire Formation: Complexities of a carbon storage system seal: Environmental Geoscience, v. 19, p. 81–104, doi:10.1306/eg.02081211014.

O'Neil, J. R., R. N. Clayton, and T. K. Mayeda, 1969, Oxygen isotope fractionation in divalent metal carbonates: Journal of Chemical Physics, v. 51, no. 12, p. 5547–5558, doi:10.1063/1.1671982.

Palkovic, M. J., 2015, Depositional characterization of the Eau Claire Formation at the Illinois Basin–Decatur Project: Facies, mineralogy and geochemistry, Master's thesis, University of Illinois at Urbana–Champaign, Urbana–Champaign, Illinois, 84 p.

Pollastro, R. M., 1985, Mineralogical and morphological evidence for the formation of illite at the expense of illite/smectite: Clays and Clay Minerals, v. 33, no. 4, p. 265–274, doi:10.1346/CCMN.1985.0330401.

Pollington, A. D., R. Kozdon, and J. W. Valley, 2011, Evolution of quartz cementation during burial of the Cambrian Mount Simon Sandstone, Illinois Basin: In situ microanalysis of $\delta^{18}O$: Geology, v. 39, no. 12, p. 1119–1122, doi:10.1130/G32195.1.

Rowan, E. L., M. B. Goldhaber, and J. R. Hatch, 2002, Regional fluid flow as a factor in the thermal history of the Illinois Basin: Constraints from fluid inclusions and the maturity of Pennsylvanian coals: AAPG Bulletin, v. 86, no. 2, p. 257–277.

Schmid, S., R. H. Worden, and Q. J. Fisher, 2004, Diagenesis and reservoir quality of the Sherwood Sandstone (Triassic), Corrib Field, Slyne Basin, west of Ireland: Marine and Petroleum Geology, v. 21, p. 299–315, doi:10.1016/j.marpetgeo.2003.11.015.

Sibley, D. F., and R. G. Gregg, 1987, Classification of dolomite rock textures: Journal of Sedimentary Petrology, v. 15, p. 1112–1114.

Śliwiński, M. G., K. Kitajima, R. Kozdon, M. J. Spicuzza, J. H. Fournelle, A. Denny, and J. W. Valley, 2015a, Secondary ion mass spectrometry bias on isotope ratios in dolomite–ankerite, part I: $\delta^{18}O$ matrix effects: Geostandards and Geoanalytical Research, doi:10.1111/j.1751-908X.2015.00364.x.

Śliwiński, M. G., K. Kitajima, R. Kozdon, M. J. Spicuzza, J. H. Fournelle, A. Denny, and J. W. Valley, 2015b, Secondary ion mass spectrometry bias on isotope ratios in dolomite–ankerite, part II: $\delta^{13}C$ matrix effects: Geostandards and Geoanalytical Research, doi:10.1111/j.1751-908X.2015.00380.x.

Śliwiński, M. G., R. Kozdon, K. Kitajima, A. Denny, M. J. Spicuzza, and J. W. Valley, 2015c, In-situ, micron-scale $\delta^{13}C$ & $\delta^{18}O$ analyses (by SIMS) of chemo-isotopically zoned carbonate cements of diagenetic origin—A case study on the implications for the thermal and burial history of the Eau Claire Fm., Illinois Basin (U.S.A.) (abs.): AAPG Annual Convention and Exhibition, Denver, Colorado, May 31–June 3, 2015, accessed October 10, 2015, http://www.searchanddiscovery.com/abstracts/html/2015/90216ace/abstracts/2097287.html.

Środoń, J., 1984, X-ray powder diffraction identification of illitic materials.: Clays and Clay Minerals, v. 32, no. 5, p. 337–349, doi:10.1346/CCMN.1984.0320501.

Surdam, R., and P. Yin, 1994, Organic acids and carbonate stability, the key to predicting positive porosity anomalies, *in* E. D. Pittman and M. D. Lewan, eds., Organic acids in geological processes: Berlin, Germany, Springer-Verlag, p. 399–448, doi:10.1007/978-3-642-78356-2_13.

Sverjensky, D. A, 1986, Genesis of Mississippi Valley–type lead-zinc deposits: Annual Review of Earth and Planetary Sciences, v. 14, p. 177–199, doi:10.1146/annurev.ea.14.050186.001141.

Swezey, C. S., 2007, Assessment of undiscovered oil and gas resources of the Illinois Basin, 2007: US Geological Survey Fact Sheet 2007-3058: Reston, Virginia, US Geological Survey, 2 p.

Swezey, C. S., 2009, Regional stratigraphy and petroleum systems of the Illinois Basin, U.S.A.: Reston, Virginia, US Geological Survey Scientific Investigations Map 3068.

US Department of Energy, 2010, Carbon sequestration atlas of the United States and Canada: National Energy Technology Laboratory, 1 sheet, accessed January 1, 2015, http://www.netl.doe.gov/research/coal/carbon-storage/natcarb-atlas.

Valley, J. W., and N. T. Kita, 2009, In situ oxygen isotope geochemistry by ion microprobe, *in* M. Fayek, ed., Secondary ion mass spectrometry in the earth sciences: Mineralogical Association of Canada Short Course 41, p. 19–63.

Vasconcelos, C., J. A. McKenzie, R. Warthmann, and S. M. Bernasconi, 2005, Calibration of the $\delta^{18}O$ paleothermometer for dolomite precipitated in microbial cultures and natural environments: Geology, v. 33, no. 4, p. 317–320, doi:10.1130/G20992.1.

Veizer, J., P. Bruckschen, F. Pawellek, A. Diener, O. G. Podlaha, G. A. F. Carden, T. Jasper, et al., 1997, Oxygen isotope evolution of Phanerozoic seawater: Palaeogeography, Palaeoclimatology, Palaeoecology, v. 132, p. 159–172, doi:10.1016/S0031-0182(97)00052-7.

Wilkinson, M., S. F. Crowley, and J. D. Marshall, 1992, Model for the evolution of oxygen isotope ratios in the pore fluids of mudrocks during burial: Marine and Petroleum Geology, v. 9, p. 98–105, doi:10.1016/0264-8172(92)90007-2.

Willman, H. B., E. Atherton, T. C. Buschbach, C. Collinson, J. C. Frye, M. E. Hopkins, J. A. Lineback, and J. A. Simon, 1975, Handbook of Illinois stratigraphy: Illinois State Geological Survey Bulletin 95, 261 p.

Wilson, T. V., and D. F. Sibley, 1978, Pressure solution and porosity reduction in shallow buried quartz arenite: AAPG Bulletin, v. 62, no. 11, p. 2329–2334.

Whitney, G., and H. R. Northrop, 1988, Experimental investigation of the smectite to illite reaction: Dual reaction mechanism and oxygen-isotope systematics: American Mineralogist, v. 73, p. 77–90.

Zartman, R. E., 1977, Geochronology of some alkali rock provinces in eastern and central United States: Annual Review of Earth and Planetary Sciences, v. 5, p. 257–286, doi:10.1146/annurev.ea.05.050177.001353.